

Topological resilience of optical skyrmions in local decoherence

Li-Wen Wang,^{1,2} Sheng Liu,^{1,2,*} Cheng-Jie Zhang,^{3,4} Geng Chen,^{1,2,4}
Yong-Sheng Zhang,^{1,2,4,†} Chuan-Feng Li,^{1,2,4} and Guang-Can Guo^{1,2,4}

¹CAS Key Laboratory of Quantum Information, University of Science and Technology of China, Hefei, 230026, China

²CAS Center for Excellence in Quantum Information and Quantum Physics,
University of Science and Technology of China, Hefei, 230026, China

³School of Physical Science and Technology, Ningbo University, Ningbo, 315211, China

⁴Hefei National Laboratory, University of Science and Technology of China, Hefei, 230088, China

(Dated: November 13, 2024)

The concept of skyrmions was introduced as early as the 1960s by Tony Skyrme. The topologically protected configuration embedded in skyrmions has prompted some investigations into their fundamental properties and versatile applications, sparking interest and guiding ongoing development. The topological protection associated with skyrmions was initially observed in systems with interactions. It is widely believed that skyrmions are stable yet relevant confirmation and empirical research remains limited. A pertinent question is whether skyrmion configurations formed by single-particle wave functions also exhibit topological stability. In this study, we affirm this hypothesis by investigating the effects of local decoherence. We analytically and numerically demonstrate the topological resilience of skyrmions and occurrence of transition points of skyrmion numbers in local decoherence of three typical decoherence channels. On the other hand, we show that these qualities are independent of the initial state. From the numerical results, we verify that inhomogeneous but continuous decoherence channels also adhere to the same behaviors and hold topological stability of skyrmions as homogeneous decoherence channels. These properties of skyrmions contribute to further applications in various areas including communication and imaging.

Introduction.—In the 1960s, Tony Skyrme introduced the concept of skyrmions primarily to describe the structure of nucleons [1, 2]. The skyrmion model proposes that nucleons are topological structures embedded in space, providing a theoretical framework to elucidate their interactions and dynamic behaviors. Thanks to their topological excitation properties, skyrmions find wide-ranging applications in fields such as condensed matter physics [3, 4], liquid crystals [5], and quantum Hall systems [6–10]. Not surprisingly, skyrmions textures can emerge in different physical systems with various mechanisms. Numerous researchers have delved into theoretical studies of magnetic skyrmions in magnetic systems and have experimentally observed their spin configurations [11, 12] with some distinctive material environments, i.e. non-centrosymmetric ferromagnets [13–17] or centrosymmetric ferromagnets combined with uniaxial anisotropy [18, 19] and even interface of ferromagnetic monolayers [20, 21].

Given the potential and significant application prospects exhibited by skyrmions, counterpart in optics is now being developed to explore analogous topological properties [22] and it has been first realized by an evanescent electromagnetic field on an interface [23, 24]. Very recently, optical skyrmionic structures in free space based on vectorial optical fields having broad utilizations can be generated and observed by a superposition of two structured light modes [25–28] with two mutually orthogonal polarizations [29–32]. Meanwhile, more advanced and sophisticated skyrmionic spin textures are revealed, such as various types of skyrmions named

bimerons and merons [22, 33, 34], momentum space skyrmions [35], space-time skyrmions with toroidal pulses [36–39] and even 3-dimensional (3D) hopfions [40].

Skyrmions have topological protected configurations and can be characterized by the corresponding topological numbers, i.e. skyrmion numbers. It is commonly believed that skyrmions are stable. Therefore, skyrmions have huge application prospects in many fields and are becoming the focus of attention due to the topological stability. A few researchers have begun to do some investigations about the robustness of skyrmions against perturbations. Liu *et al.* investigated the robustness of optical skyrmions against disorder from random fluctuations in amplitude and phase of the field [41]. Ornelas *et al.* demonstrated experimentally the topological resilience of optical skyrmions to entanglement decay by an amplitude damping operation [42]. However, the empirical research in this important area still remains relatively scarce. And all these impressive advances do not further explore the robustness of skyrmions in the context of local decoherence. A comprehensive understanding of skyrmions in local decoherence is supposed to be crucial and indispensable for their practical applications, including communication, information encoding and imaging.

Here, we consider three typical decoherence channels and an optical skyrmion field constructed by structured light carrying orbital angular momentum (OAM) with two orthogonal polarizations [30, 43] to study different topological properties and stability of skyrmions while the light field propagates through different noisy channels. We explore more general scenarios beyond

merely considering pure states and report the topological resilience of skyrmions in local decoherence.

Background.—A 2-dimensional (2D) skyrmion can be regarded as a mapping from the 2D transverse spatial plane onto a Bloch sphere or a Poincaré sphere with 4π solid angle [42]. In general, a skyrmion is expressed simply as a state $|\Psi(\mathbf{r})\rangle = \psi_1(\mathbf{r})|0\rangle + \psi_2(\mathbf{r})|1\rangle$, and $\psi_{1,2}(\mathbf{r})$ are transverse spatial modes, $|0\rangle = \begin{pmatrix} 1 \\ 0 \end{pmatrix}$ and $|1\rangle = \begin{pmatrix} 0 \\ 1 \end{pmatrix}$ represent two mutually orthogonal vectors.

And this statement applies to two-level systems. In this paper, we consider optical skyrmion fields in free space and take paraxial Laguerre-Gaussian (LG) beams $\psi_{m,l}(\mathbf{r})$ carrying OAM as transverse spatial modes with two orthogonal polarization states. This types of skyrmionic beams can be described by [30]

$$|\Psi(\mathbf{r})\rangle = a\psi_{l_1}(\mathbf{r})|0\rangle + b\psi_{l_2}(\mathbf{r})|1\rangle, \quad (1)$$

where the radial index $m = 0$, $|a|^2 + |b|^2 = 1$, and $|0\rangle$ and $|1\rangle$ can be regarded as horizontal polarization $|H\rangle$ and vertical polarization $|V\rangle$ in the optical field. For convenience and conciseness, the state in Eq. (1) can be written in a general form $|\Psi\rangle = a|l_1\rangle|0\rangle + b|l_2\rangle|1\rangle$ involving two degrees of freedom (DOFs) of a particle, where $|l\rangle = \int_{\mathcal{R}^2} |\psi_l(\mathbf{r})|e^{il\phi} |\mathbf{r}\rangle d\mathbf{r}$.

For a skyrmionic beam, we need to introduce the normalized local Stokes parameters [44], a three-component vector $\mathbf{S}(\mathbf{r}) = \langle S_x(\mathbf{r}), S_y(\mathbf{r}), S_z(\mathbf{r}) \rangle (S_x^2 + S_y^2 + S_z^2 = 1)$, to define this skyrmion field and point in the spin direction. We should note that the normalization of Stokes parameters is necessary in general cases. Here, the three components of Stokes parameters correspond to the expected values of three Pauli operators in the local normalized state, i.e. $S_j(\mathbf{r}) = \langle \sigma_j \rangle(\mathbf{r}) = \frac{I_i^+(\mathbf{r}) - I_i^-(\mathbf{r})}{I_i^+(\mathbf{r}) + I_i^-(\mathbf{r})}$, where $i = x, y, z$ and $I_i^\pm(\mathbf{r}) = |\langle \lambda_i^\pm | \Psi(\mathbf{r}) \rangle|^2$ are the projection intensities of the state $|\Psi(\mathbf{r})\rangle$ on the eigenstates $|\lambda_i^\pm\rangle$ related to the eigenvalues $\lambda_i^\pm = \pm 1$ of the Pauli operator σ_i ($\sigma_x = |0\rangle\langle 1| + |1\rangle\langle 0|$, $\sigma_y = -i|0\rangle\langle 1| + i|1\rangle\langle 0|$ and $\sigma_z = |0\rangle\langle 0| - |1\rangle\langle 1|$).

To characterize the topological nature of the optical skyrmion field, a topological number, also known as the skyrmion number, is required. The skyrmion number indicates the number of times the 2D transverse plane \mathcal{R}^2 wraps around a unit sphere \mathcal{S}^2 . The expression of the skyrmion number is

$$N_z = \frac{1}{4\pi} \int_{\mathcal{R}^2} \mathbf{S} \cdot \frac{\partial \mathbf{S}}{\partial x} \times \frac{\partial \mathbf{S}}{\partial y} dx dy. \quad (2)$$

To understand the topological stability of skyrmions in local decoherence, we employ three typical decoherence channels acting on a single qubit, i.e., phase damping channel, depolarizing channel and amplitude damping channel [45, 46]. These channels are non-unitary processes for systems and lead to loss of information

and degradation of state [47], which allow specific representations via corresponding Kraus operators. We assume that this channel map is described by the notation E and the output density matrix of this system is

$$\rho_{out} = E(\rho) = \sum_{\nu} K_{\nu} \rho K_{\nu}^{\dagger}, \quad (3)$$

where K is the Kraus operator satisfying $\sum_{\nu} K_{\nu}^{\dagger} K_{\nu} = \mathbb{I}$ and ρ is the input density matrix of the system.

When an input state passes through a phase damping channel, its output form is

$$\rho_{out} = \left(1 - \frac{p_1}{2}\right) \rho + \frac{p_1}{2} (\mathbb{I} \otimes \sigma_z) \rho (\mathbb{I} \otimes \sigma_z), \quad (4)$$

where $p_1 \in [0, 1]$ and $p_1 = 0$ denotes that the system remains unaffected. Here, \mathbb{I} is an identify operator on the spatial wave function. Phase damping channel can destroy the off-diagonal term of the state while the diagonal term remains intact.

The depolarizing channel can be supposed to be most unbiased decoherence way and has a unique symmetry of state degradation since the probability of each error is equal. The density matrix is

$$\begin{aligned} \rho_{out} = (1 - p_2) \rho + \frac{p_2}{3} [& (\mathbb{I} \otimes \sigma_x) \rho (\mathbb{I} \otimes \sigma_x) \\ & + (\mathbb{I} \otimes \sigma_y) \rho (\mathbb{I} \otimes \sigma_y) + (\mathbb{I} \otimes \sigma_z) \rho (\mathbb{I} \otimes \sigma_z)]. \end{aligned} \quad (5)$$

where $p_2 \in [0, \frac{3}{4}]$ and $p_2 = 0$ suggests that the error probability is 0, while $p_2 \in (\frac{3}{4}, 1]$ is non-physical.

The Kraus operators of amplitude damping channel [46, 48, 49] are

$$K_0 = \begin{pmatrix} 1 & 0 \\ 0 & \sqrt{\eta} \end{pmatrix}, K_1 = \begin{pmatrix} 0 & \sqrt{1-\eta} \\ 0 & 0 \end{pmatrix}, \eta \in [0, 1]. \quad (6)$$

η represents the transmission coefficient, showing perfect transmission in $\eta = 1$ and complete amplitude damping in $\eta = 0$. The diagonal and off-diagonal terms of the state will be both affected by this channel, so it can cause the dissipation and decoherence of the state. The output state is expressed as

$$\rho_{out} = (\mathbb{I} \otimes K_0) \rho (\mathbb{I} \otimes K_0^{\dagger}) + (\mathbb{I} \otimes K_1) \rho (\mathbb{I} \otimes K_1^{\dagger}). \quad (7)$$

More details of the above three channels can be found in Appendix.

Results.—We analytically and numerically calculate skyrmion numbers of optical skyrmion fields that propagate in different local decoherence channels. Intriguingly, the interplay between topology and coherence is remarkably subtle, showing the topological resilience of skyrmions. As an optical skyrmion field traverses a decoherence channel, we derive the density matrix and Stokes parameters of the system. By assuming beam propagation in the z -direction, we

compute the z -component of the skyrmions field, thereby revealing the corresponding skyrmion number. It is noteworthy that the Stokes parameters equivalently indicate the direction of the effective magnetization and are solely related to the pointing angle. Therefore, it is essential to normalize them so that the normalized Stokes parameters lie on the unit sphere [44].

Considering LG spatial modes with radial index $m = 0$ and the input state in Eq. (1), for simplicity, we express the complicated formulas $\psi_{l_1}(\mathbf{r})$ and $\psi_{l_2}(\mathbf{r})$ in a concise form

$$v(\mathbf{r}) = v(r, \phi, z) = \frac{b\psi_{l_2}(\mathbf{r})}{a\psi_{l_1}(\mathbf{r})} = A(z)r^{|l_2|-|l_1|}e^{i\Delta l\phi}, \quad (8)$$

where $A(z)$ is a complex expression containing z and $\Delta l = |l_2 - l_1|$ with $l_1 \neq -l_2$. We get the analytical solutions of skyrmion numbers in different local decoherence channels as follows:

$$\text{Phase damping channel : } N_z^{\text{PDC}} = \begin{cases} \Delta l, & 0 \leq p_1 < 1 \\ 0, & p_1 = 1 \end{cases}. \quad (9)$$

$$\text{Depolarizing channel : } N_z^{\text{DC}} = \begin{cases} \Delta l, & 0 \leq p_2 < \frac{3}{4} \\ 0, & p_2 = \frac{3}{4} \end{cases}. \quad (10)$$

$$\text{Amplitude damping channel : } N_z^{\text{ADC}} = \begin{cases} \Delta l, & \frac{1}{2} < \eta \leq 1 \\ 0, & 0 \leq \eta < \frac{1}{2} \end{cases}, \quad (11)$$

where $\eta \neq \frac{1}{2}$ in Eq. (11). More details are in Appendix.

In Eq. (9), we know that skyrmion numbers are not affected by phase local decoherence unless $p_1 = 1$ revealing complete phase damping. In this case, the corresponding Stokes parameters are $\mathbf{S}(\mathbf{r}) = \langle (1 - p_1)S_x(\mathbf{r}), (1 - p_1)S_y(\mathbf{r}), S_z(\mathbf{r}) \rangle$. As the damping factor p_1 is close to 1, the two components $S_x(\mathbf{r})$ and $S_y(\mathbf{r})$ approach 0 while $S_z(\mathbf{r})$ holds unchanged, producing the effect that the coherence between the two components of the optical skyrmion field gradually disappears and finally the output is a maximal mixed state. Therefore, topological stability is maintained as long as coherence is preserved, as shown in Fig. 1(a).

For depolarizing channel, due to the final Stokes parameters are in proportion to the initial values, i.e. $\mathbf{S}(\mathbf{r}) = (1 - \frac{4p_2}{3})\langle S_x(\mathbf{r}), S_y(\mathbf{r}), S_z(\mathbf{r}) \rangle$, the Stokes parameters after being normalized in local decoherence are identical and invariant except for the case of $p_2 = \frac{3}{4}$. Therefore, we have the analytical solution in Eq. (10) and the skyrmion number remains constant related to Δl (when $p_2 \neq \frac{3}{4}$). The illustration is in Fig. 1(b).

We can see that the occurrence of transition points of the first two channels are similar to the one in Ref. [42] showing the absence of non-trivial topology of skyrmions once the entanglement vanishes. In the case of amplitude damping channel, we can find that it differs from the

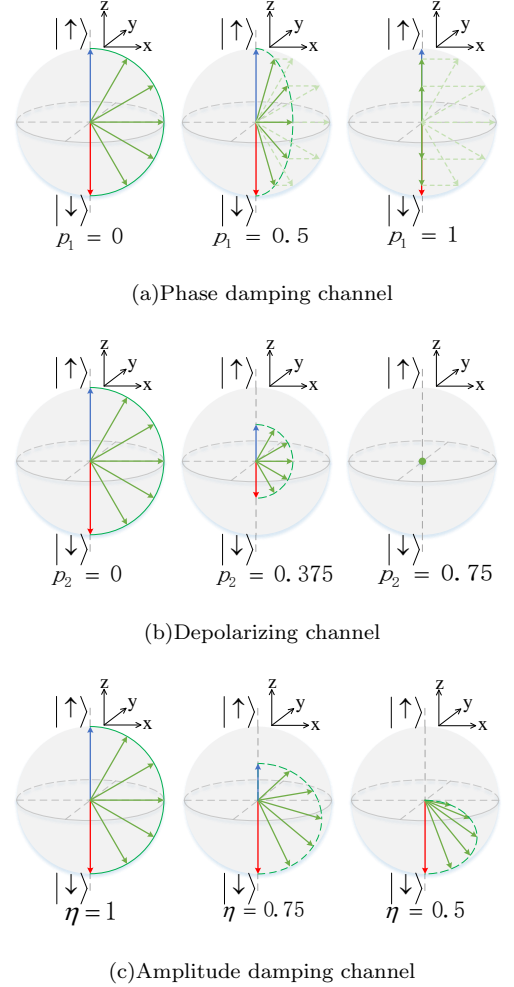


FIG. 1. Diagrams of the spin vector change on the Bloch sphere after passing through the decoherence channel. The normalized Stokes parameters $\mathbf{S}(\mathbf{r}) = \langle S_x(\mathbf{r}), S_y(\mathbf{r}), S_z(\mathbf{r}) \rangle = (\sin \theta \cos \phi, \sin \theta \sin \phi, \cos \theta)$ (polar angle: $\theta \in [0, \pi]$; azimuthal angle: $\phi \in [0, 2\pi]$), denote the unit vector on the Bloch sphere. We take a slice ($S_y = 0$ i.e. azimuth $\phi = 0$) on the Bloch sphere as an example to observe the changes of spin vectors. **(a)** Phase damping channel: With the damping factor p_1 of PDC increases, S_x and S_y gradually decreases, whereas S_z remains unchanged. Once $p_1 = 1$, all the spin vectors will fall on the central axis and it is a maximal mixed state without coherence. **(b)** Depolarizing channel: As the damping factor p_2 of DC decreases, the three components of the Stokes parameters will proportionately contract towards the center of the sphere, eventually converging to a single point. **(c)** Amplitude damping channel: When $\eta = 1$, spin vectors can cover the whole Bloch sphere. When $\eta \in (\frac{1}{2}, 1)$ (like $\eta = 0.75$), S_x decreases and the magnitude of the blue spin vector pointing to the North Pole is reduced to half of its initial value. When $\eta = 0.5$, the blue spin vector vanishes and there are only spin vectors for the southern hemisphere.

above and $\eta = \frac{1}{2}$ is the transition point of skyrmion numbers and skyrmion numbers hold invariant as long as the damping factor satisfies the condition $\eta \in (\frac{1}{2}, 1]$.

We explain this phenomenon as follows. The amplitude damping channel demonstrates a process of the decay of two-level (atom) system due to the spontaneous emission. $\{|1\rangle, |0\rangle\}$ can be seen as the upper energy level (the excited state) and the lower energy level (the ground state) of this system, and initial populations are $|b|^2$ and $|a|^2$, respectively. There is a probability $1 - \eta$ of decaying from the excited state to the ground state so that final populations become $\eta|b|^2$ and $|a|^2 + (1 - \eta)|b|^2$. As η decreases, the population of the upper level gradually decreases. When $\eta \leq \frac{1}{2}$, the inequality $\eta|b|^2 \leq |a|^2 + (1 - \eta)|b|^2$ is always true. It is well-known that skyrmions is a mapping from \mathcal{R}^2 to \mathcal{S}^2 containing the whole 4π solid angle, however, it will only map half of the Bloch sphere and topological spin textures will also be destroyed once $\eta \leq \frac{1}{2}$, as shown in Fig. 1(c).

Meanwhile, we numerically demonstrate the results that the normalized skyrmion numbers vary with damping factors in three local decoherence channels in Fig. 2. Here, we consider that initial scale coefficients satisfy $a = b = \frac{1}{\sqrt{2}}$ and the azimuthal indices of two OAM modes are $l_1 = 8$ and $l_2 = 0$. It is obvious that these numerical results in Fig. 2(a), 2(b) and 2(c) (represented by curves with hollow circles in blue) are in good agreement with the analytic solutions in Eq. (9), (10) and (11). Additionally, Eq. (8) shows that the occurrence of these transition points is independent of the initial state. Apart from the case of maximum entanglement (i.e. $a = b = \frac{1}{\sqrt{2}}$), as long as $a \neq 0$ and $b \neq 0$, all trends hold.

Compared the skyrmion number with the entanglement degree between two DOFs characterized by a quantity named concurrence [50–52], there is evidence that the skyrmion number does not change entirely synchronously with entanglement during local decoherence. We obtain the analytical formulas about concurrence in three channels in the following

$$C^{\text{PDC}}(\rho_{out}) = 2|a||b|(1 - p_1), p_1 \in [0, 1], \quad (12)$$

$$C^{\text{DC}}(\rho_{out}) = \max\{2|a||b|(1 - 2p_2), 0\}, p_2 \in [0, \frac{3}{4}], \quad (13)$$

$$C^{\text{ADC}}(\rho_{out}) = 2|a||b|\sqrt{\eta}, \eta \in [0, 1]. \quad (14)$$

And the numerical curves of concurrence in Fig. 2 is perfectly fitted with theoretical values. In phase damping channel and amplitude damping channel, the concurrence approaches zero when complete coherence damping occurs, as shown in Fig. 2(a) and 2(c). For depolarizing channel in Fig. 2(b), however, it behaves very differently. The concurrence goes to 0 prematurely, a phenomenon known as entanglement sudden death [53–57], which describes the complete loss of quantum correlation (or entanglement) in a finite time rather than an asymptotic decay over an infinite duration. More details are in Appendix. As shown in Fig. 2, due to the presence of transition points of skyrmion numbers,

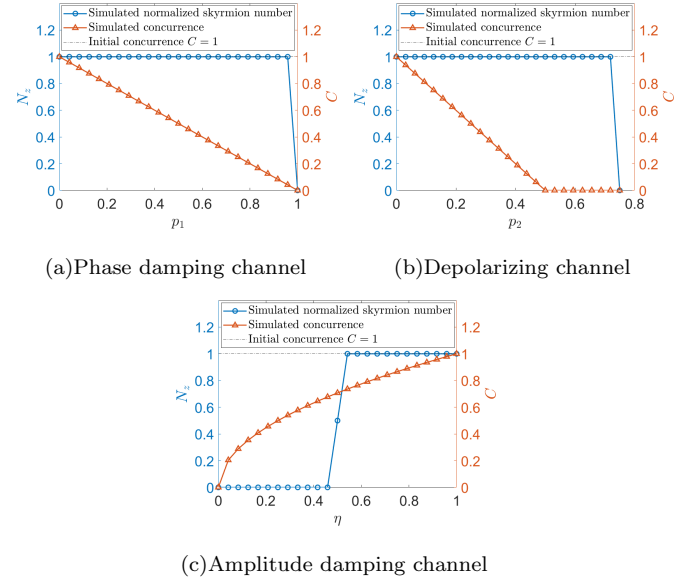


FIG. 2. Normalized skyrmion numbers and relevant concurrence. Blue curves with hollow circles represent simulated normalized skyrmion numbers, corresponding orange curves with plus signs represent simulated concurrence values, and black dotted lines are initial concurrence values (here it is $C = 1$ with $a = b = \frac{1}{\sqrt{2}}$). **(a)** Phase damping channel: the damping factor p corresponds to $p_1 \in [0, 1]$. **(b)** Depolarizing channel: the damping factor p corresponds to $p_2 \in [0, \frac{3}{4}]$. **(c)** Amplitude damping channel: the damping factor is $\eta \in [0, 1]$.

the skyrmion number is more robust than concurrence in these cases.

Intensity loss of two polarization components is also an aspect to consider and we can characterize the loss by two loss parameters $T_a \in [0, 1]$ and $T_b \in [0, 1]$. In fact, the loss parameters have no influence on the stability of skyrmion numbers unless at least one component is lose completely. Because the variations of loss parameters T_a and T_b are equivalent to the variations of the scale coefficients a and b . More details can be found in Appendix.

All of the above studies are based on a homogeneous decoherence process, where the damping factors are uniformly distributed in space (i.e. a constant). Extending this investigation, we find that the topological resilience of an optical skyrmion field propagating through an inhomogeneous yet continuous local decoherence channel still persists. We numerically generate an inhomogeneous local decoherence channel, where the damping factor varies randomly across the spatial domain and the correlation of damping factors between any two positions is characterized by a specific correlation length ϵ [58]. The continuity of damping factors of the channel is supposed to be guaranteed by increasing the correlation length ϵ because the skyrmion numbers are unaffected by the operations of smooth deformations [42]. The numerical grid size

is 1024×1024 . Consequently, when $\epsilon = 1024$, the inhomogeneous channel deteriorates into a homogeneous one. The results are shown in Tab. I and we perform 50 realizations for the ensemble average on account of the existence of random process. Similarly to the uniform case, we confirm numerically that the skyrmion numbers remain stable and the topology is preserved in these instances: (1) $p_1(\mathbf{r}) \in [0, 1]$ in phase damping channel; (2) $p_2(\mathbf{r}) \in [0, 3/4]$ in depolarizing channel; (3) $\eta(\mathbf{r}) \in (1/2, 1]$ and $\epsilon > 2$ (the continuity of the channel is better) in amplitude damping channel. More details are in Appendix.

$N_z^{\text{sim}}/N_z^{\text{the}}$	Type			
		PDC	DC	ADC
ϵ (grids)				
1		0.9986	1.0000	0.9186
2		0.9999	1.0000	0.9589
4		1.0000	1.0000	0.9849
8		1.0000	1.0000	0.9964
16		1.0000	1.0000	0.9993
32		1.0000	1.0000	1.0000
64		1.0000	1.0000	1.0000
128		0.9998	1.0000	1.0000
256		0.9995	1.0000	1.0000
512		0.9966	1.0000	1.0000

TABLE I. Normalized skyrmion numbers in the inhomogeneous local decoherence channels with different types and different correlation lengths ϵ in units of a single grid point. N_z^{sim} is the simulated skyrmion number and N_z^{the} is the theoretical skyrmion number. For phase damping channel, the damping factor $p_1(\mathbf{r}) \in [0, 1]$; For depolarizing channel, the damping factor $p_2(\mathbf{r}) \in [0, 3/4]$; For amplitude damping channel, the damping factor $\eta(\mathbf{r}) \in (1/2, 1]$.

Discussion and conclusion.—We have investigated the topological resilience of skyrmions in three local decoherence scenarios. Both analytically and numerically, we have proven the validity of this topological property. By considering a 2D optical skyrmion field constructed by paraxial LG spatial modes with two orthogonal polarization states, we have found that the two skyrmion numbers N_z^{PDC} and N_z^{DC} in phasing noise and depolarizing noise maintain invariant unless their damping factors p_1 and p_2 reach their respective maximum values indicating completely damping. Moreover, as the decoherence strength increasing, the skyrmion number N_z^{ADC} remains topologically stable until the damping factor η of amplitude noise is less than or equal to $\frac{1}{2}$, which means that the topological spin texture is destroyed and the mapping from \mathcal{R}^2 to \mathcal{S}^2 is also incomplete. The immunity against local decoherence endowed by skyrmions' topology is independent of the scale coefficients (a, b) and spatial modes' azimuthal indices (l_1, l_2) of the initial state. Due to the existence of transition points of skyrmion numbers in local decoherence, the skyrmion numbers are more robust than the concurrence in these

cases. And we also demonstrate numerically that these features are still valid for inhomogeneous yet continuous decoherence channels.

In this paper, we consider two DOFs of a particle to create the optical skyrmion field. The analysis is not restricted by this condition, and our results continue to be applicable to common systems (two-level single-particle or two-level single-particle ensemble system), inspiring additional generalization among skyrmions in optics and magnetism. Meanwhile, compared with the pure states and unitary channels in Ref. [27, 42], we employ more general expressions and non-unitary channels to study the stability of skyrmion numbers. The robustness of skyrmion numbers can be used to guide the transmission of classical discrete signals. It is expected that topological resilience in local decoherence has greater application prospects in more research fields, including communication, information encoding and processing, metrology and imaging.

Note added.—We notice that there is a similar work [59] when our paper is in preparation. Our work differs from the work in Ref [59]: we consider single-particle systems rather than entangled bi-photon states. Our findings are applicable to classical optical fields and can be generalized to other physical systems, as long as the noise in those systems is localized.

Acknowledgments.—This work was supported by the National Natural Science Foundation of China (No. 92065113), Innovation Program for Quantum Science and technology (No. 2021ZD0301201) and the University Synergy Innovation Program of Anhui Province (No. GXXT-2022-039).

* shengliu@ustc.edu.cn

† yshzhang@ustc.edu.cn

- [1] T. H. R. Skyrme and B. F. J. Schonland, Proceedings of the Royal Society of London. Series A. Mathematical and Physical Sciences **260**, 127 (1961).
- [2] T. Skyrme, Nuclear Phys. **31**, 556 (1962).
- [3] A. N. Bogdanov and C. Panagopoulos, Nature Rev. Phys. **2**, 492 (2020).
- [4] C. Wang, C. Gao, C.-M. Jian, and H. Zhai, Phys. Rev. Lett. **105**, 160403 (2010).
- [5] T. Nagase, M. Komatsu, Y. G. So, T. Ishida, H. Yoshida, Y. Kawaguchi, Y. Tanaka, K. Saitoh, N. Ikarashi, M. Kuwahara, and M. Nagao, Phys. Rev. Lett. **123**, 137203 (2019).
- [6] Y. Taguchi, Y. Oohara, H. Yoshizawa, N. Nagaosa, and Y. Tokura, Science **291**, 2573 (2001).
- [7] A. Neubauer, C. Pfleiderer, B. Binz, A. Rosch, R. Ritz, P. G. Niklowitz, and P. Böni, Phys. Rev. Lett. **102**, 186602 (2009).
- [8] C. Pfleiderer and A. Rosch, Nature **465**, 880 (2010).
- [9] R. Ritz, M. Halder, M. Wagner, C. Franz, A. Bauer, and C. Pfleiderer, Nature **497**, 231 (2013).
- [10] M. Mochizuki, X. Yu, S. Seki, N. Kanazawa,

- W. Koshibae, J. Zang, M. Mostovoy, Y. Tokura, and N. Nagaosa, *Nature Materials* **13**, 241 (2014).
- [11] A. Fert, N. Reyren, and V. Cros, *Nature Rev. Materials* **2**, 1 (2017).
- [12] X. Zhang, Y. Zhou, K. M. Song, T.-E. Park, J. Xia, M. Ezawa, X. Liu, W. Zhao, G. Zhao, and S. Woo, *J. of Phys.: Condensed Matter* **32**, 143001 (2020).
- [13] A. N. Bogdanov and D. Yablonskii, *Zh. Eksp. Teor. Fiz* **95**, 178 (1989).
- [14] A. Bogdanov and A. Hubert, *Journal of Magnetism and Magnetic Materials* **138**, 255 (1994).
- [15] U. K. Roessler, A. Bogdanov, and C. Pfleiderer, *Nature* **442**, 797 (2006).
- [16] S. Mühlbauer, B. Binz, F. Jonietz, C. Pfleiderer, A. Rosch, A. Neubauer, R. Georgii, and P. Böni, *Science* **323**, 915 (2009).
- [17] X. Yu, Y. Onose, N. Kanazawa, J. H. Park, J. Han, Y. Matsui, N. Nagaosa, and Y. Tokura, *Nature* **465**, 901 (2010).
- [18] T. Garel and S. Doniach, *Phys. Rev. B* **26**, 325 (1982).
- [19] A. P. Malozemoff and J. C. Slonczewski, *Magnetic domain walls in bubble materials: advances in materials and device research*, Vol. 1 (Academic press, 2013).
- [20] S. Heinze, K. Von Bergmann, M. Menzel, J. Brede, A. Kubetzka, R. Wiesendanger, G. Bihlmayer, and S. Blügel, *Nature Phys.* **7**, 713 (2011).
- [21] N. Romming, C. Hanneken, M. Menzel, J. E. Bickel, B. Wolter, K. von Bergmann, A. Kubetzka, and R. Wiesendanger, *Science* **341**, 636 (2013).
- [22] Y. Shen, Q. Zhang, P. Shi, L. Du, X. Yuan, and A. V. Zayats, *Nature Photonics* **18**, 15 (2024).
- [23] S. Tsesses, E. Ostrovsky, K. Cohen, B. Gjonaj, N. Lindner, and G. Bartal, *Science* **361**, 993 (2018).
- [24] L. Du, A. Yang, A. V. Zayats, and X. Yuan, *Nature Phys.* **15**, 650 (2019).
- [25] C. Rosales-Guzmán, B. Ndagano, and A. Forbes, *J. of Optics* **20**, 123001 (2018).
- [26] Z. Wan, H. Wang, Q. Liu, X. Fu, and Y. Shen, *ACS Photonics* **10**, 2149 (2023).
- [27] I. Nape, K. Singh, A. Klug, W. Buono, C. Rosales-Guzman, A. McWilliam, S. Franke-Arnold, A. Kritzinger, P. Forbes, A. Dudley, and A. Forbes, *Nature Photonics* **16**, 538 (2022).
- [28] C. Peters, M. Cox, A. Drozdov, and A. Forbes, *Appl. Phys. Lett.* **123** (2023).
- [29] C. He, Y. Shen, and A. Forbes, *Light: Science & Applications* **11**, 205 (2022).
- [30] S. Gao, F. C. Speirits, F. Castellucci, S. Franke-Arnold, S. M. Barnett, and J. B. Götte, *Phys. Rev. A* **102**, 053513 (2020).
- [31] R. Gutiérrez-Cuevas and E. Pisanty, *J. of Optics* **23**, 024004 (2021).
- [32] Y. Shen, E. C. Martínez, and C. Rosales-Guzmán, *ACS Photonics* **9**, 296 (2022).
- [33] X. Lei, A. Yang, P. Shi, Z. Xie, L. Du, A. V. Zayats, and X. Yuan, *Phys. Rev. Lett.* **127**, 237403 (2021).
- [34] H. Jani, J.-C. Lin, J. Chen, J. Harrison, F. Maccherozzi, J. Schad, S. Prakash, C.-B. Eom, A. Ariando, T. Venkatesan, and P. G. Radaelli, *Nature* **590**, 74 (2021).
- [35] C. Guo, M. Xiao, Y. Guo, L. Yuan, and S. Fan, *Phys. Rev. Lett.* **124**, 106103 (2020).
- [36] A. Zdagkas, C. McDonnell, J. Deng, Y. Shen, G. Li, T. Ellenbogen, N. Papasimakis, and N. I. Zheludev, *Nature Photonics* **16**, 523 (2022).
- [37] Y. Shen, N. Papasimakis, and N. I. Zheludev, *Nature Commun.* **15**, 4863 (2024).
- [38] R. Wang, D.-T. Yang, T. Xin, S. Shi, B.-Z. Wang, and Y. Shen, *Appl. Phys. Lett.* **125** (2024).
- [39] R. Wang, P.-Y. Bao, Z.-Q. Hu, S. Shi, B.-Z. Wang, N. I. Zheludev, and Y. Shen, *Appl. Phys. Rev.* **11** (2024).
- [40] Y. Shen, B. Yu, H. Wu, C. Li, Z. Zhu, and A. V. Zayats, *Adv. Photonics* **5**, 015001 (2023).
- [41] C. Liu, S. Zhang, S. A. Maier, and H. Ren, *Phys. Rev. Lett.* **129**, 267401 (2022).
- [42] P. Ornelas, I. Nape, R. de Mello Koch, and A. Forbes, *Nature Photonics* **18**, 258 (2024).
- [43] J. Zhu, S. Liu, Y.-S. Zhang, C.-F. Li, and G.-C. Guo, *Phys. Rev. A* **110**, 043522 (2024).
- [44] S. Seki and M. Mochizuki, *Skyrmions in magnetic materials*, Vol. 10 (Springer, 2016).
- [45] J. Preskill, *California Institute of Technology* **16**, 1 (1998).
- [46] A. Cuevas, M. Proietti, M. A. Ciampini, S. Duranti, P. Mataloni, M. F. Sacchi, and C. Macchiavello, *Phys. Rev. Lett.* **119**, 100502 (2017).
- [47] G. Narang, S. Dogra, and Arvind, *Quant. Infor. Proc.* **19**, 1 (2020).
- [48] A. Cuevas, A. Mari, A. De Pasquale, A. Orieux, M. Massaro, F. Sciarrino, P. Mataloni, and V. Giovannetti, *Phys. Rev. A* **96**, 012314 (2017).
- [49] T. Yu and J. H. Eberly, *Phys. Rev. B* **68**, 165322 (2003).
- [50] S. A. Hill and W. K. Wootters, *Phys. Rev. Lett.* **78**, 5022 (1997).
- [51] W. K. Wootters, *Phys. Rev. Lett.* **80**, 2245 (1998).
- [52] T. Yu and J. H. Eberly, *Phys. Rev. Lett.* **93**, 140404 (2004).
- [53] T. Yu and J. H. Eberly, *Phys. Rev. Lett.* **97**, 140403 (2006).
- [54] M. P. Almeida, F. de Melo, M. Hor-Meyll, A. Salles, S. Walborn, P. S. Ribeiro, and L. Davidovich, *Science* **316**, 579 (2007).
- [55] W. Cui, Z. Xi, and Y. Pan, *J. of Phys. A* **42**, 025303 (2008).
- [56] T. Yu and J. Eberly, *Science* **323**, 598 (2009).
- [57] Y. Meng, S. Yu, Z.-A. Jia, Y.-T. Wang, Z.-J. Ke, W. Liu, Z.-P. Li, Y.-Z. Yang, H. Wang, Y.-C. Wu, J.-S. Tang, C.-F. Li, and G.-C. Guo, *Phys. Rev. A* **102**, 042415 (2020).
- [58] J. W. Goodman, *Speckle phenomena in optics: theory and applications* (Roberts and Company Publishers, 2007).
- [59] R. d. M. Koch, B.-Q. Lu, P. Ornelas, I. Nape, and A. Forbes, *arXiv:2410.23789* (2024).
- [60] K. Yashodamma, P. Geetha, and Sudha, *Quant. Infor. Proc.* **13**, 2551 (2014).
- [61] R. Bavontaweepanya, in *Journal of Physics: Conference Series*, Vol. 1144 (IOP Publishing, 2018) p. 012047.
- [62] D. D. Duncan and S. J. Kirkpatrick, in *Complex dynamics and fluctuations in biomedical photonics V*, Vol. 6855 (SPIE, 2008) pp. 23–30.

APPENDIX

Skyrmion numbers N_z

Skyrmions are a type of topological spin textures characterized by corresponding topological numbers, i.e. skyrmion numbers. For the electron spin, the normalized local magnetization $\mathbf{m}(\mathbf{r})$ defines the relevant skyrmion field. In turn, for the light beam, a normalized Stokes vector is introduced to calculate the skyrmion number. An optical skyrmion can be regarded as a mapping from a transverse spatial plane \mathcal{R}^2 to a Poincaré sphere (or a Bloch sphere in spin) \mathcal{S}^2 , which has a two-dimensional (2D) surface of a three-dimensional (3D) ball and completely covers a 4π solid angle, and the skyrmion number denotes the number of times of \mathcal{R}^2 wrapping \mathcal{S}^2 . The i th component of the skyrmion field can be expressed by [30]

$$\Sigma_i = \frac{1}{2} \epsilon_{ijk} \epsilon_{pqr} S_p \frac{\partial S_q}{\partial x_j} \frac{\partial S_r}{\partial x_k}, \quad (\text{S1})$$

where the notations ϵ_{ijk} and ϵ_{pqr} are both Levi-civita symbols and the subscript $i = x, y, z$. Nevertheless, we only need to exploit the z th component Σ_z

$$\begin{aligned} \Sigma_z(x, y) &= \frac{1}{2} \epsilon_{pqr} S_p \frac{\partial S_q}{\partial x} \frac{\partial S_r}{\partial y} - \frac{1}{2} \epsilon_{pqr} S_p \frac{\partial S_q}{\partial y} \frac{\partial S_r}{\partial x} \\ &= S_x \left(\frac{\partial S_y}{\partial x} \frac{\partial S_z}{\partial y} - \frac{\partial S_z}{\partial x} \frac{\partial S_y}{\partial y} \right) \\ &\quad + S_y \left(\frac{\partial S_z}{\partial x} \frac{\partial S_x}{\partial y} - \frac{\partial S_x}{\partial x} \frac{\partial S_z}{\partial y} \right) \\ &\quad + S_z \left(\frac{\partial S_x}{\partial x} \frac{\partial S_y}{\partial y} - \frac{\partial S_y}{\partial x} \frac{\partial S_x}{\partial y} \right) \\ &= \mathbf{S} \cdot \left(\frac{\partial \mathbf{S}}{\partial x} \times \frac{\partial \mathbf{S}}{\partial y} \right), \end{aligned} \quad (\text{S2})$$

where S_i is spatially distributed, i.e. $S_i(x, y)$. Therefore, the skyrmion number is described as [30]

$$N_z = \frac{1}{4\pi} \iint \Sigma_z(x, y) dx dy. \quad (\text{S3})$$

Stokes parameters $\mathbf{S}(\mathbf{r})$

To calculate skyrmion numbers, we need to obtain relevant Stokes parameters and this operation is also called Stokes measurements. The input state of this system is written in the general form $|\Psi\rangle = a |l_1\rangle |0\rangle + b |l_2\rangle |1\rangle$, where $|l\rangle = \int_{\mathcal{R}^2} |\psi_l(\mathbf{r})| e^{il\phi} |\mathbf{r}\rangle d\mathbf{r}$ and $\{|0\rangle, |1\rangle\}$ are two mutually orthogonal states. Here, we consider paraxial Laguerre-Gaussian (LG) modes with no radial index ($m = 0$) and the $\psi_{m,l}(\mathbf{r})$ is described as

$$\begin{aligned} \psi_{m,l}(r, \phi, z) &= \frac{C_{ml}}{w(z)} \left[\frac{\sqrt{2}r}{w(z)} \right]^{|l|} L_m^{|l|} \left[\frac{2r^2}{w^2(z)} \right] \exp \left[-\frac{r^2}{w^2(z)} \right] \exp(il\phi) \\ &\quad \times \exp \left[\frac{-ikr^2 z}{2(z^2 + z_R^2)} \right] \exp \left[i(2m + |l| + 1) \arctan \left(\frac{z}{z_R} \right) \right], \end{aligned} \quad (\text{S4})$$

where $C_{ml} = \sqrt{\frac{2m!}{\pi(m+|l|)!}}$ is a normalization constant, $L_m^{|l|}(x)$ is the generalized Laguerre polynomial, $z_R = \frac{\pi w_0^2}{\lambda}$ is the Rayleigh distance, λ represents the beam wavelength, w_0 is the beam waist of the fundamental mode, and $w(z) = w_0 \sqrt{1 + \left(\frac{z}{z_R} \right)^2}$ is the beam radius at the z plane.

The initial density matrix is

$$\begin{aligned}
\rho &= |\Psi\rangle \langle \Psi| \\
&= |a|^2 |l_1\rangle \langle l_1| \otimes |0\rangle \langle 0| + ab^* |l_1\rangle \langle l_2| \otimes |0\rangle \langle 1| \\
&\quad + a^*b |l_2\rangle \langle l_1| \otimes |1\rangle \langle 0| + |b|^2 |l_2\rangle \langle l_2| \otimes |1\rangle \langle 1| \\
&= \sum_{pqst=1}^2 \mu_{pqst} |l_p\rangle \langle l_q| \otimes |e_s\rangle \langle e_t|,
\end{aligned} \tag{S5}$$

where $|e_1\rangle = |0\rangle$, $|e_2\rangle = |1\rangle$, $\mu_{1111} = |a|^2$, $\mu_{1212} = ab^*$, $\mu_{2121} = a^*b$, $\mu_{2222} = |b|^2$, and other coefficients are zero. The Stokes parameters correspond to the expected values of measurement operators of the overall system, i.e.

$$S_{j=x,y,z}(\mathbf{r}) = \langle \mathbf{r} | \langle \mathbf{r} | \otimes \sigma_j = \text{Tr}(\mathbf{r}) \langle \mathbf{r} | \otimes \sigma_j \rho, \tag{S6}$$

where $\text{Tr}(\cdot)$ is the trace operator, the position basis of orbital angular momentum (OAM) degree of freedom (DOF) $\{|\mathbf{r}\rangle, \mathbf{r} \in \mathcal{R}^2\}$ satisfies the orthogonality $\langle \mathbf{r}_1 | \mathbf{r}_2 \rangle = \delta(\mathbf{r}_1 - \mathbf{r}_2)$ and the completeness relation $\int_{\mathcal{R}^2} |\mathbf{r}\rangle \langle \mathbf{r}| d\mathbf{r} = \mathbb{I}$. By employing Eq. (S5) into Eq. (S6), we can get

$$\begin{aligned}
S_{j=x,y,z}(\mathbf{r}) &= \sum_{pqst=1}^2 \mu_{pqst} \text{Tr}(|\mathbf{r}\rangle \langle \mathbf{r}| l_p \langle l_q|) \text{Tr}(\sigma_j |e_s\rangle \langle e_t|) \\
&= \sum_{pqst=1}^2 \mu_{pqst} \langle \mathbf{r} | l_p \rangle \langle l_q | \mathbf{r} \rangle \text{Tr}(\sigma_j |e_s\rangle \langle e_t|) \\
&= \sum_{pqst=1}^2 \mu_{pqst} \psi_{l_p}(\mathbf{r}) \psi_{l_q}^*(\mathbf{r}) \text{Tr}(\sigma_j |e_s\rangle \langle e_t|),
\end{aligned} \tag{S7}$$

where $\langle \mathbf{r} | l \rangle = \psi_l(\mathbf{r})$. For the term $\text{Tr}(\sigma_j |e_s\rangle \langle e_t|)$, we can rewrite it by the eigenvalue decomposition method, i.e. $\sigma_j = \lambda_j^+ P_j^+ + \lambda_j^- P_j^-$. So Eq. (S7) can be expressed by

$$\begin{aligned}
S_{j=x,y,z}(\mathbf{r}) &= \lambda_j^+ \sum_{pqst=1}^2 \mu_{pqst} \psi_{l_p}(\mathbf{r}) \psi_{l_q}^*(\mathbf{r}) \langle e_t | P_j^+ | e_s \rangle \\
&\quad + \lambda_j^- \sum_{pqst=1}^2 \mu_{pqst} \psi_{l_p}(\mathbf{r}) \psi_{l_q}^*(\mathbf{r}) \langle e_t | P_j^- | e_s \rangle,
\end{aligned} \tag{S8}$$

where $\lambda_j^\pm = \pm 1$ and P_j^\pm are the projection operators. Therefore, we can calculate the three locally normalized Stokes components of the initial density matrix in detail.

$$\tilde{S}_x(\mathbf{r}) = \frac{I_D(\mathbf{r}) - I_A(\mathbf{r})}{I_D(\mathbf{r}) + I_A(\mathbf{r})}, \tag{S9}$$

$$\tilde{S}_y(\mathbf{r}) = \frac{I_R(\mathbf{r}) - I_L(\mathbf{r})}{I_R(\mathbf{r}) + I_L(\mathbf{r})}, \tag{S10}$$

$$\tilde{S}_z(\mathbf{r}) = \frac{I_H(\mathbf{r}) - I_V(\mathbf{r})}{I_H(\mathbf{r}) + I_V(\mathbf{r})}, \tag{S11}$$

where $I_k(\mathbf{r}) = I |\langle k | \langle \mathbf{r} | \Psi \rangle|^2 = I [\text{Tr}(|\mathbf{r}\rangle \langle \mathbf{r}| \otimes |k\rangle \langle k| \rho)]$ ($k = D, A, R, L, H, V$), and I is the total intensity in the skyrmionic beam. In fact, $I_k(\mathbf{r})$ is the first or second term of Eq. (S8) after the eigenvalues are removed. These states $\{|D\rangle, |A\rangle, |R\rangle, |L\rangle, |H\rangle, |V\rangle\}$ are the eigenvectors of three Pauli operators $\{\sigma_x, \sigma_y, \sigma_z\}$, respectively. ($|D\rangle = 1/\sqrt{2}(|0\rangle + |1\rangle)$, $|A\rangle = 1/\sqrt{2}(|0\rangle - |1\rangle)$, $|R\rangle = 1/\sqrt{2}(|0\rangle + i|1\rangle)$, $|L\rangle = 1/\sqrt{2}(|0\rangle - i|1\rangle)$, $|H\rangle = |0\rangle$, $|V\rangle = |1\rangle$.) Each $I_k(\mathbf{r})$ is

$$\begin{aligned}
I_D(\mathbf{r}) &= \frac{1}{2} \mu_{1111} \psi_{l_1}(\mathbf{r}) \psi_{l_1}^*(\mathbf{r}) + \frac{1}{2} \mu_{1212} \psi_{l_1}(\mathbf{r}) \psi_{l_2}^*(\mathbf{r}) \\
&\quad + \frac{1}{2} \mu_{2121} \psi_{l_2}(\mathbf{r}) \psi_{l_1}^*(\mathbf{r}) + \frac{1}{2} \mu_{2222} \psi_{l_2}(\mathbf{r}) \psi_{l_2}^*(\mathbf{r}),
\end{aligned} \tag{S12}$$

$$\begin{aligned}
I_A(\mathbf{r}) &= \frac{1}{2}\mu_{1111}\psi_{l_1}(\mathbf{r})\psi_{l_1}^*(\mathbf{r}) - \frac{1}{2}\mu_{1212}\psi_{l_1}(\mathbf{r})\psi_{l_2}^*(\mathbf{r}) \\
&\quad - \frac{1}{2}\mu_{2121}\psi_{l_2}(\mathbf{r})\psi_{l_1}^*(\mathbf{r}) + \frac{1}{2}\mu_{2222}\psi_{l_2}(\mathbf{r})\psi_{l_2}^*(\mathbf{r}),
\end{aligned} \tag{S13}$$

$$\begin{aligned}
I_R(\mathbf{r}) &= \frac{1}{2}\mu_{1111}\psi_{l_1}(\mathbf{r})\psi_{l_1}^*(\mathbf{r}) + \frac{i}{2}\mu_{1212}\psi_{l_1}(\mathbf{r})\psi_{l_2}^*(\mathbf{r}) \\
&\quad - \frac{i}{2}\mu_{2121}\psi_{l_2}(\mathbf{r})\psi_{l_1}^*(\mathbf{r}) + \frac{1}{2}\mu_{2222}\psi_{l_2}(\mathbf{r})\psi_{l_2}^*(\mathbf{r}),
\end{aligned} \tag{S14}$$

$$\begin{aligned}
I_L(\mathbf{r}) &= \frac{1}{2}\mu_{1111}\psi_{l_1}(\mathbf{r})\psi_{l_1}^*(\mathbf{r}) - \frac{i}{2}\mu_{1212}\psi_{l_1}(\mathbf{r})\psi_{l_2}^*(\mathbf{r}) \\
&\quad + \frac{i}{2}\mu_{2121}\psi_{l_2}(\mathbf{r})\psi_{l_1}^*(\mathbf{r}) + \frac{1}{2}\mu_{2222}\psi_{l_2}(\mathbf{r})\psi_{l_2}^*(\mathbf{r}),
\end{aligned} \tag{S15}$$

$$I_H(\mathbf{r}) = \mu_{1111}\psi_{l_1}(\mathbf{r})\psi_{l_1}^*(\mathbf{r}), \tag{S16}$$

$$I_V(\mathbf{r}) = \mu_{2222}\psi_{l_2}(\mathbf{r})\psi_{l_2}^*(\mathbf{r}). \tag{S17}$$

Substituting Eq. (S12)-(S17) into Eq. (S9)-(S11), we can obtain the final forms of locally normalized Stokes parameters

$$\tilde{S}_x(\mathbf{r}) = \frac{2 \operatorname{Re}[ab^*\psi_{l_1}(\mathbf{r})\psi_{l_2}^*(\mathbf{r})]}{|a|^2|\psi_{l_1}(\mathbf{r})|^2 + |b|^2|\psi_{l_2}(\mathbf{r})|^2}, \tag{S18}$$

$$\tilde{S}_y(\mathbf{r}) = \frac{-2 \operatorname{Im}[ab^*\psi_{l_1}(\mathbf{r})\psi_{l_2}^*(\mathbf{r})]}{|a|^2|\psi_{l_1}(\mathbf{r})|^2 + |b|^2|\psi_{l_2}(\mathbf{r})|^2}, \tag{S19}$$

$$\tilde{S}_z(\mathbf{r}) = \frac{|a|^2|\psi_{l_1}(\mathbf{r})|^2 - |b|^2|\psi_{l_2}(\mathbf{r})|^2}{|a|^2|\psi_{l_1}(\mathbf{r})|^2 + |b|^2|\psi_{l_2}(\mathbf{r})|^2}. \tag{S20}$$

And the three elements satisfy the vector normalization relation $\tilde{S}_x^2 + \tilde{S}_y^2 + \tilde{S}_z^2 = 1$.

Analytical solutions of skyrmion numbers in local decoherence

We primarily consider three decoherence channels, i.e., phase damping channel, depolarizing channel and amplitude damping channel. The decoherence channels are solely acting on the polarization DOF and OAM DOF maintains unaffected by imposing on an identity operator \mathbb{I} . We use Kraus operators $\{K_\nu\}$ to characterize these channels.

A. Phase damping channel

For phase damping channel, the output state is

$$\rho_{\text{PDC}} = E(\rho) = \left(1 - \frac{p_1}{2}\right)\rho + \frac{p_1}{2}(\mathbb{I} \otimes \sigma_z)\rho(\mathbb{I} \otimes \sigma_z), \tag{S21}$$

and this channel can be related by the Kraus operators $K_0 = \sqrt{1-p_1}\mathbb{I}$, $K_1 = \sqrt{p_1}\begin{pmatrix} 1 & 0 \\ 0 & 0 \end{pmatrix}$, $K_2 = \sqrt{p_1}\begin{pmatrix} 0 & 0 \\ 0 & 1 \end{pmatrix}$, $p_1 \in [0, 1]$. Kraus operators have the property of $\sum_\nu K_\nu^\dagger K_\nu = \mathbb{I}$. If we input a density matrix of a single qubit $\rho_i = \begin{pmatrix} \rho_{00} & \rho_{01} \\ \rho_{10} & \rho_{11} \end{pmatrix}$, the output density matrix after the channel is

$$\rho_o = \begin{pmatrix} \rho_{00} & (1-p_1)\rho_{01} \\ (1-p_1)\rho_{10} & \rho_{11} \end{pmatrix}. \tag{S22}$$

The final density matrix of the phase damping channel is (from the initial state in Eq. (S5))

$$\rho_{\text{PDC}} = \sum_{pqst=1}^2 \mu'_{pqst} |l_p\rangle \langle l_q| \otimes |e_s\rangle \langle e_t|, \quad (\text{S23})$$

where $\mu'_{1111} = |a|^2$, $\mu'_{1212} = (1-p_1)ab^*$, $\mu'_{2121} = (1-p_1)a^*b$, $\mu'_{2222} = |b|^2$, and other coefficients are zero. The locally normalized Stokes parameters are

$$\begin{aligned} \tilde{S}_x^{\text{PDC}}(\mathbf{r}) &= \frac{(1-p_1) \cdot 2 \operatorname{Re}[ab^* \psi_{l_1}(\mathbf{r}) \psi_{l_2}^*(\mathbf{r})]}{\sqrt{[|a|^2 |\psi_{l_1}(\mathbf{r})|^2 + |b|^2 |\psi_{l_2}(\mathbf{r})|^2]^2 - 4p_1(2-p_1)|a|^2 |b|^2 |\psi_{l_1}(\mathbf{r})|^2 |\psi_{l_2}(\mathbf{r})|^2}} \\ &= \frac{(1-p_1)[v(\mathbf{r}) + v^*(\mathbf{r})]}{\sqrt{[1 + |v(\mathbf{r})|^2]^2 - 4p_1(2-p_1)|v(\mathbf{r})|^2}}, \end{aligned} \quad (\text{S24})$$

$$\begin{aligned} \tilde{S}_y^{\text{PDC}}(\mathbf{r}) &= \frac{-(1-p_1) \cdot 2 \operatorname{Im}[ab^* \psi_{l_1}(\mathbf{r}) \psi_{l_2}^*(\mathbf{r})]}{\sqrt{[|a|^2 |\psi_{l_1}(\mathbf{r})|^2 + |b|^2 |\psi_{l_2}(\mathbf{r})|^2]^2 - 4p_1(2-p_1)|a|^2 |b|^2 |\psi_{l_1}(\mathbf{r})|^2 |\psi_{l_2}(\mathbf{r})|^2}} \\ &= \frac{-i(1-p_1)[v(\mathbf{r}) - v^*(\mathbf{r})]}{\sqrt{[1 + |v(\mathbf{r})|^2]^2 - 4p_1(2-p_1)|v(\mathbf{r})|^2}}, \end{aligned} \quad (\text{S25})$$

$$\begin{aligned} \tilde{S}_z^{\text{PDC}}(\mathbf{r}) &= \frac{|a|^2 |\psi_{l_1}(\mathbf{r})|^2 - |b|^2 |\psi_{l_2}(\mathbf{r})|^2}{\sqrt{[|a|^2 |\psi_{l_1}(\mathbf{r})|^2 + |b|^2 |\psi_{l_2}(\mathbf{r})|^2]^2 - 4p_1(2-p_1)|a|^2 |b|^2 |\psi_{l_1}(\mathbf{r})|^2 |\psi_{l_2}(\mathbf{r})|^2}} \\ &= \frac{1 - |v(\mathbf{r})|^2}{\sqrt{[1 + |v(\mathbf{r})|^2]^2 - 4p_1(2-p_1)|v(\mathbf{r})|^2}}. \end{aligned} \quad (\text{S26})$$

The equality $\tilde{S}_x^2 + \tilde{S}_y^2 + \tilde{S}_z^2 = 1$ must be fulfilled and we simplify the two LG spatial modes ($\psi_{l_1}(\mathbf{r})$ and $\psi_{l_2}(\mathbf{r})$) into the following form

$$v(\mathbf{r}) = v(r, \phi, z) = \frac{b\psi_{l_2}(\mathbf{r})}{a\psi_{l_1}(\mathbf{r})} = A(z)r^{|l_2|-|l_1|} e^{i\Delta l \phi}, \quad (\text{S27})$$

where $\Delta l = |l_2 - l_1|$.

In the polar coordinate $\{r, \phi, z\}$, we can get

$$\begin{aligned} \frac{\partial \tilde{S}_x^{\text{PDC}}}{\partial x} &= \cos \phi \frac{\partial \tilde{S}_x^{\text{PDC}}}{\partial r} - \frac{1}{r} \sin \phi \frac{\partial \tilde{S}_x^{\text{PDC}}}{\partial \phi} \\ &= \frac{(1-p_1)}{rB_1} \{ \cos \phi (|l_2| - |l_1|) (v + v^*) [B_1^2 \\ &\quad - 2|v|^2(1 + |v|^2 - 2p_1(2-p_1))]/B_1^2 - i \sin \phi \Delta l (v - v^*) \}, \end{aligned} \quad (\text{S28})$$

$$\begin{aligned} \frac{\partial \tilde{S}_x^{\text{PDC}}}{\partial y} &= \sin \phi \frac{\partial \tilde{S}_x^{\text{PDC}}}{\partial r} + \frac{1}{r} \cos \phi \frac{\partial \tilde{S}_x^{\text{PDC}}}{\partial \phi} \\ &= \frac{(1-p_1)}{rB_1} \{ \sin \phi (|l_2| - |l_1|) (v + v^*) [B_1^2 \\ &\quad - 2|v|^2(1 + |v|^2 - 2p_1(2-p_1))]/B_1^2 + i \cos \phi \Delta l (v - v^*) \}, \end{aligned} \quad (\text{S29})$$

$$\begin{aligned} \frac{\partial \tilde{S}_y^{\text{PDC}}}{\partial x} &= \cos \phi \frac{\partial \tilde{S}_y^{\text{PDC}}}{\partial r} - \frac{1}{r} \sin \phi \frac{\partial \tilde{S}_y^{\text{PDC}}}{\partial \phi} \\ &= -\frac{i(1-p_1)}{rB_1} \{ \cos \phi (|l_2| - |l_1|) (v - v^*) [B_1^2 \\ &\quad - 2|v|^2(1 + |v|^2 - 2p_1(2-p_1))]/B_1^2 - i \sin \phi \Delta l (v + v^*) \}, \end{aligned} \quad (\text{S30})$$

$$\begin{aligned}
\frac{\partial \tilde{S}_y^{\text{PDC}}}{\partial y} &= \sin \phi \frac{\partial \tilde{S}_y^{\text{PDC}}}{\partial r} + \frac{1}{r} \cos \phi \frac{\partial \tilde{S}_y^{\text{PDC}}}{\partial \phi} \\
&= -\frac{i(1-p_1)}{rB_1} \{ \sin \phi (|l_2| - |l_1|)(v - v^*) [B_1^2 \\
&\quad - 2|v|^2(1 + |v|^2 - 2p_1(2 - p_1))] / B_1^2 + i \cos \phi \Delta l (v + v^*) \},
\end{aligned} \tag{S31}$$

$$\begin{aligned}
\frac{\partial \tilde{S}_z^{\text{PDC}}}{\partial x} &= \cos \phi \frac{\partial \tilde{S}_z^{\text{PDC}}}{\partial r} - \frac{1}{r} \sin \phi \frac{\partial \tilde{S}_z^{\text{PDC}}}{\partial \phi} \\
&= -\frac{2(|l_2| - |l_1|)|v|^2}{rB_1^3} \{ \cos \phi [B_1^2 + (1 - |v|^2)(1 + |v|^2 - 2p_1(2 - p_1))] \},
\end{aligned} \tag{S32}$$

$$\begin{aligned}
\frac{\partial \tilde{S}_z^{\text{PDC}}}{\partial y} &= \sin \phi \frac{\partial \tilde{S}_z^{\text{PDC}}}{\partial r} + \frac{1}{r} \cos \phi \frac{\partial \tilde{S}_z^{\text{PDC}}}{\partial \phi} \\
&= -\frac{2(|l_2| - |l_1|)|v|^2}{rB_1^3} \{ \sin \phi [B_1^2 + (1 - |v|^2)(1 + |v|^2 - 2p_1(2 - p_1))] \},
\end{aligned} \tag{S33}$$

where $B_1^2 = (1 + |v|^2)^2 - 4p_1(2 - p_1)|v|^2$. The relevant z th component of the field and the skyrmion number respectively are

$$\Sigma_z^{\text{PDC}} = \frac{4\Delta l (|l_2| - |l_1|)|v|^2}{r^2} \cdot \frac{(1 - p_1)(1 + |v|^2)}{[(1 + |v|^2)^2 - 4p_1(2 - p_1)|v|^2]^{3/2}}, \tag{S34}$$

$$N_z^{\text{PDC}} = \begin{cases} \Delta l, & 0 \leq p_1 < 1 \\ 0, & p_1 = 1 \end{cases} \tag{S35}$$

B. Depolarizing channel

For depolarizing channel, the output state is

$$\rho_{\text{DC}} = E(\rho) = (1 - p_2) \rho + \frac{p_2}{3} [(\mathbb{I} \otimes \sigma_x) \rho (\mathbb{I} \otimes \sigma_x) + (\mathbb{I} \otimes \sigma_y) \rho (\mathbb{I} \otimes \sigma_y) + (\mathbb{I} \otimes \sigma_z) \rho (\mathbb{I} \otimes \sigma_z)], \tag{S36}$$

and the Kraus operators of this channel are

$$K_0 = \sqrt{1 - p_2} \mathbb{I}, K_1 = \sqrt{\frac{p_2}{3}} \begin{pmatrix} 0 & 1 \\ 1 & 0 \end{pmatrix}, K_2 = \sqrt{\frac{p_2}{3}} \begin{pmatrix} 0 & -i \\ i & 0 \end{pmatrix}, K_3 = \sqrt{\frac{p_2}{3}} \begin{pmatrix} 1 & 0 \\ 0 & -1 \end{pmatrix}, p_2 \in [0, \frac{3}{4}]. \tag{S37}$$

If we input a density matrix of a single qubit $\rho_i = \begin{pmatrix} \rho_{00} & \rho_{01} \\ \rho_{10} & \rho_{11} \end{pmatrix}$, the output density matrix after the channel is

$$\rho_o = \begin{pmatrix} (1 - \frac{2p_2}{3})\rho_{00} + \frac{2p_2}{3}\rho_{11} & (1 - \frac{4p_2}{3})\rho_{01} \\ (1 - \frac{4p_2}{3})\rho_{10} & (1 - \frac{2p_2}{3})\rho_{11} + \frac{2p_2}{3}\rho_{00} \end{pmatrix}. \tag{S38}$$

The final density matrix of the depolarizing channel is

$$\rho_{\text{DC}} = \sum_{pqst=1}^2 \mu''_{pqst} |l_p\rangle \langle l_q| \otimes |e_s\rangle \langle e_t|, \tag{S39}$$

where $\mu''_{1111} = (1 - \frac{2p_2}{3})|a|^2$, $\mu''_{1212} = (1 - \frac{4p_2}{3})ab^*$, $\mu''_{2121} = (1 - \frac{4p_2}{3})a^*b$, $\mu''_{2222} = (1 - \frac{2p_2}{3})|b|^2$, $\mu''_{2211} = \frac{2p_2}{3}|b|^2$, $\mu''_{1122} = \frac{2p_2}{3}|a|^2$, and other coefficients are zero. The Stokes parameters in depolarizing channel differ only by a factor $(1 - \frac{4p_2}{3})$ from the Stokes parameters in the input state, and this factor has no effect after vector normalization.

Thereby the locally normalized Stokes parameters in depolarizing channel are the same as Eq. (S18), (S19) and (S20):

$$\begin{aligned}\tilde{S}_x^{\text{DC}}(\mathbf{r}) &= \frac{2 \operatorname{Re}[ab^* \psi_{l_1}(\mathbf{r}) \psi_{l_2}^*(\mathbf{r})]}{|a|^2 |\psi_{l_1}(\mathbf{r})|^2 + |b|^2 |\psi_{l_2}(\mathbf{r})|^2} \\ &= \frac{v(\mathbf{r}) + v^*(\mathbf{r})}{1 + |v(\mathbf{r})|^2},\end{aligned}\quad (\text{S40})$$

$$\begin{aligned}\tilde{S}_y^{\text{DC}}(\mathbf{r}) &= \frac{-2 \operatorname{Im}[ab^* \psi_{l_1}(\mathbf{r}) \psi_{l_2}^*(\mathbf{r})]}{|a|^2 |\psi_{l_1}(\mathbf{r})|^2 + |b|^2 |\psi_{l_2}(\mathbf{r})|^2} \\ &= \frac{-i[v(\mathbf{r}) - v^*(\mathbf{r})]}{1 + |v(\mathbf{r})|^2},\end{aligned}\quad (\text{S41})$$

$$\begin{aligned}\tilde{S}_z^{\text{DC}}(\mathbf{r}) &= \frac{|a|^2 |\psi_{l_1}(\mathbf{r})|^2 - |b|^2 |\psi_{l_2}(\mathbf{r})|^2}{|a|^2 |\psi_{l_1}(\mathbf{r})|^2 + |b|^2 |\psi_{l_2}(\mathbf{r})|^2} \\ &= \frac{1 - |v(\mathbf{r})|^2}{1 + |v(\mathbf{r})|^2}.\end{aligned}\quad (\text{S42})$$

Here, $\tilde{S}_x^2 + \tilde{S}_y^2 + \tilde{S}_z^2 = 1$ and $v(\mathbf{r}) = v(r, \phi, z) = \frac{b \psi_{l_2}(\mathbf{r})}{a \psi_{l_1}(\mathbf{r})} = A(z) r^{|l_2| - |l_1|} e^{i \Delta l \phi}$, where $\Delta l = |l_2 - l_1|$.

Then

$$\begin{aligned}\frac{\partial \tilde{S}_x^{\text{DC}}}{\partial x} &= \cos \phi \frac{\partial \tilde{S}_x^{\text{DC}}}{\partial r} - \frac{1}{r} \sin \phi \frac{\partial \tilde{S}_x^{\text{DC}}}{\partial \phi} \\ &= \frac{1}{r(1 + |v|^2)} \{ \cos \phi (|l_2| - |l_1|) (v + v^*) (1 - |v|^2) / (1 + |v|^2) - i \sin \phi \Delta l (v - v^*) \},\end{aligned}\quad (\text{S43})$$

$$\begin{aligned}\frac{\partial \tilde{S}_x^{\text{DC}}}{\partial y} &= \sin \phi \frac{\partial \tilde{S}_x^{\text{DC}}}{\partial r} + \frac{1}{r} \cos \phi \frac{\partial \tilde{S}_x^{\text{DC}}}{\partial \phi} \\ &= \frac{1}{r(1 + |v|^2)} \{ \sin \phi (|l_2| - |l_1|) (v + v^*) (1 - |v|^2) / (1 + |v|^2) + i \cos \phi \Delta l (v - v^*) \},\end{aligned}\quad (\text{S44})$$

$$\begin{aligned}\frac{\partial \tilde{S}_y^{\text{DC}}}{\partial x} &= \cos \phi \frac{\partial \tilde{S}_y^{\text{DC}}}{\partial r} - \frac{1}{r} \sin \phi \frac{\partial \tilde{S}_y^{\text{DC}}}{\partial \phi} \\ &= -\frac{i}{r(1 + |v|^2)} \{ \cos \phi (|l_2| - |l_1|) (v - v^*) (1 - |v|^2) / (1 + |v|^2) - i \sin \phi \Delta l (v + v^*) \},\end{aligned}\quad (\text{S45})$$

$$\begin{aligned}\frac{\partial \tilde{S}_y^{\text{DC}}}{\partial y} &= \sin \phi \frac{\partial \tilde{S}_y^{\text{DC}}}{\partial r} + \frac{1}{r} \cos \phi \frac{\partial \tilde{S}_y^{\text{DC}}}{\partial \phi} \\ &= -\frac{i}{r(1 + |v|^2)} \{ \sin \phi (|l_2| - |l_1|) (v - v^*) (1 - |v|^2) / (1 + |v|^2) + i \cos \phi \Delta l (v + v^*) \},\end{aligned}\quad (\text{S46})$$

$$\begin{aligned}\frac{\partial \tilde{S}_z^{\text{DC}}}{\partial x} &= \cos \phi \frac{\partial \tilde{S}_z^{\text{DC}}}{\partial r} - \frac{1}{r} \sin \phi \frac{\partial \tilde{S}_z^{\text{DC}}}{\partial \phi} \\ &= -\frac{4}{r(1 + |v|^2)} \{ \cos \phi (|l_2| - |l_1|) |v|^2 / (1 + |v|^2) \},\end{aligned}\quad (\text{S47})$$

$$\begin{aligned}\frac{\partial \tilde{S}_z^{\text{DC}}}{\partial y} &= \sin \phi \frac{\partial \tilde{S}_z^{\text{DC}}}{\partial r} + \frac{1}{r} \cos \phi \frac{\partial \tilde{S}_z^{\text{DC}}}{\partial \phi} \\ &= -\frac{4}{r(1 + |v|^2)} \{ \sin \phi (|l_2| - |l_1|) |v|^2 / (1 + |v|^2) \}.\end{aligned}\quad (\text{S48})$$

The relevant z th component of the field and the skyrmion number respectively are

$$\Sigma_z^{\text{DC}} = \frac{4\Delta l(|l_2| - |l_1|)|v|^2}{r^2} \cdot \frac{1}{(1 + |v|^2)^2}, \quad (\text{S49})$$

$$N_z^{\text{DC}} = \begin{cases} \Delta l, & 0 \leq p_2 < \frac{3}{4} \\ 0, & p_2 = \frac{3}{4} \end{cases} \quad (\text{S50})$$

C. Amplitude damping channel

For amplitude damping channel, the Kraus operators are

$$K_0 = \begin{pmatrix} 1 & 0 \\ 0 & \sqrt{\eta} \end{pmatrix}, K_1 = \begin{pmatrix} 0 & \sqrt{1-\eta} \\ 0 & 0 \end{pmatrix}, \eta \in [0, 1]. \quad (\text{S51})$$

η is the damping factor. If we input a density matrix of a single qubit $\rho_i = \begin{pmatrix} \rho_{00} & \rho_{01} \\ \rho_{10} & \rho_{11} \end{pmatrix}$, the output density matrix after the channel is

$$\rho_o = \begin{pmatrix} \rho_{00} + (1-\eta)\rho_{11} & \sqrt{\eta}\rho_{01} \\ \sqrt{\eta}\rho_{10} & \eta\rho_{11} \end{pmatrix}. \quad (\text{S52})$$

The initial state in Eq. (S5) goes through an amplitude damping channel, the final state can be presented by

$$\rho_{\text{ADC}} = \sum_{pqst=1}^2 \mu'''_{pqst} |l_p\rangle \langle l_q| \otimes |e_s\rangle \langle e_t|, \quad (\text{S53})$$

where $\mu'''_{1111} = |a|^2$, $\mu'''_{2211} = (1-\eta)|b|^2$, $\mu'''_{1212} = \sqrt{\eta}ab^*$, $\mu'''_{2121} = \sqrt{\eta}a^*b$, $\mu'''_{2222} = \eta|b|^2$, and other coefficients are zero. The locally normalized Stokes parameters are

$$\tilde{S}_x^{\text{ADC}}(\mathbf{r}) = \frac{\sqrt{\eta} \cdot 2 \text{Re}[ab^* \psi_{l_1}(\mathbf{r}) \psi_{l_2}^*(\mathbf{r})]}{\sqrt{[|a|^2 |\psi_{l_1}(\mathbf{r})|^2 + |b|^2 |\psi_{l_2}(\mathbf{r})|^2]^2 - 4\eta(1-\eta)|b|^4 |\psi_{l_2}(\mathbf{r})|^4}}, \quad (\text{S54})$$

$$\tilde{S}_y^{\text{ADC}}(\mathbf{r}) = \frac{-\sqrt{\eta} \cdot 2 \text{Im}[ab^* \psi_{l_1}(\mathbf{r}) \psi_{l_2}^*(\mathbf{r})]}{\sqrt{[|a|^2 |\psi_{l_1}(\mathbf{r})|^2 + |b|^2 |\psi_{l_2}(\mathbf{r})|^2]^2 - 4\eta(1-\eta)|b|^4 |\psi_{l_2}(\mathbf{r})|^4}}, \quad (\text{S55})$$

$$\tilde{S}_z^{\text{ADC}}(\mathbf{r}) = \frac{|a|^2 |\psi_{l_1}(\mathbf{r})|^2 - (2\eta - 1) |b|^2 |\psi_{l_2}(\mathbf{r})|^2}{\sqrt{[|a|^2 |\psi_{l_1}(\mathbf{r})|^2 + |b|^2 |\psi_{l_2}(\mathbf{r})|^2]^2 - 4\eta(1-\eta)|b|^4 |\psi_{l_2}(\mathbf{r})|^4}}. \quad (\text{S56})$$

Similarly, the equality $\tilde{S}_x^2 + \tilde{S}_y^2 + \tilde{S}_z^2 = 1$ must be fulfilled. Furthermore, we simplify the two LG spatial modes ($\psi_{l_1}(\mathbf{r})$ and $\psi_{l_2}(\mathbf{r})$) into $v(\mathbf{r}) = v(r, \phi, z) = \frac{b\psi_{l_2}(\mathbf{r})}{a\psi_{l_1}(\mathbf{r})} = A(z)r^{|l_2|-|l_1|}e^{i\Delta l\phi}$, where $\Delta l = |l_2 - l_1|$. From it, we know that the specific values of scale coefficients a and b have no impact on the calculation of skyrmion numbers ($a \neq 0, b \neq 0$). After that, Eq. (S54)-(S56) can be simplified to

$$\tilde{S}_x^{\text{ADC}}(\mathbf{r}) = \frac{\sqrt{\eta}[v(\mathbf{r}) + v^*(\mathbf{r})]}{\sqrt{[1 + |v(\mathbf{r})|^2]^2 - 4\eta(1-\eta)|v(\mathbf{r})|^4}}, \quad (\text{S57})$$

$$\tilde{S}_y^{\text{ADC}}(\mathbf{r}) = \frac{-i\sqrt{\eta}[v(\mathbf{r}) - v^*(\mathbf{r})]}{\sqrt{[1 + |v(\mathbf{r})|^2]^2 - 4\eta(1-\eta)|v(\mathbf{r})|^4}}, \quad (\text{S58})$$

$$\tilde{S}_z^{\text{ADC}}(\mathbf{r}) = \frac{1 - (2\eta - 1)|v(\mathbf{r})|^2}{\sqrt{[1 + |v(\mathbf{r})|^2]^2 - 4\eta(1-\eta)|v(\mathbf{r})|^4}}. \quad (\text{S59})$$

Then

$$\begin{aligned} \frac{\partial \tilde{S}_x^{\text{ADC}}}{\partial x} &= \cos \phi \frac{\partial \tilde{S}_x^{\text{ADC}}}{\partial r} - \frac{1}{r} \sin \phi \frac{\partial \tilde{S}_x^{\text{ADC}}}{\partial \phi} \\ &= \frac{\sqrt{\eta}}{rB_2} \{ \cos \phi (|l_2| - |l_1|) (v + v^*) [B_2^2 \\ &\quad - 2|v|^2(1 + (2\eta - 1)^2|v|^2)] / B_2^2 - i \sin \phi \Delta l (v - v^*) \}, \end{aligned} \quad (\text{S60})$$

$$\begin{aligned}
\frac{\partial \tilde{S}_x^{\text{ADC}}}{\partial y} &= \sin \phi \frac{\partial \tilde{S}_x^{\text{ADC}}}{\partial r} + \frac{1}{r} \cos \phi \frac{\partial \tilde{S}_x^{\text{ADC}}}{\partial \phi} \\
&= \frac{\sqrt{\eta}}{r B_2} \{ \sin \phi (|l_2| - |l_1|) (v + v^*) [B_2^2 \\
&\quad - 2|v|^2 (1 + (2\eta - 1)^2 |v|^2)] / B_2^2 + i \cos \phi \Delta l (v - v^*) \},
\end{aligned} \tag{S61}$$

$$\begin{aligned}
\frac{\partial \tilde{S}_y^{\text{ADC}}}{\partial x} &= \cos \phi \frac{\partial \tilde{S}_y^{\text{ADC}}}{\partial r} - \frac{1}{r} \sin \phi \frac{\partial \tilde{S}_y^{\text{ADC}}}{\partial \phi} \\
&= -\frac{i\sqrt{\eta}}{r B_2} \{ \cos \phi (|l_2| - |l_1|) (v - v^*) [B_2^2 \\
&\quad - 2|v|^2 (1 + (2\eta - 1)^2 |v|^2)] / B_2^2 - i \sin \phi \Delta l (v + v^*) \},
\end{aligned} \tag{S62}$$

$$\begin{aligned}
\frac{\partial \tilde{S}_y^{\text{ADC}}}{\partial y} &= \sin \phi \frac{\partial \tilde{S}_y^{\text{ADC}}}{\partial r} + \frac{1}{r} \cos \phi \frac{\partial \tilde{S}_y^{\text{ADC}}}{\partial \phi} \\
&= -\frac{i\sqrt{\eta}}{r B_2} \{ \sin \phi (|l_2| - |l_1|) (v - v^*) [B_2^2 \\
&\quad - 2|v|^2 (1 + (2\eta - 1)^2 |v|^2)] / B_2^2 + i \sin \phi \Delta l (v + v^*) \},
\end{aligned} \tag{S63}$$

$$\begin{aligned}
\frac{\partial \tilde{S}_z^{\text{ADC}}}{\partial x} &= \cos \phi \frac{\partial \tilde{S}_z^{\text{ADC}}}{\partial r} - \frac{1}{r} \sin \phi \frac{\partial \tilde{S}_z^{\text{ADC}}}{\partial \phi} \\
&= \cos \phi \frac{2(|l_2| - |l_1|)|v|^2}{r B_2^3} [(1 - 2\eta)B_2^2 + (2\eta - 1)^3 |v|^4 - 2(2\eta - 1)(\eta - 1)|v|^2 - 1],
\end{aligned} \tag{S64}$$

$$\begin{aligned}
\frac{\partial \tilde{S}_z^{\text{ADC}}}{\partial y} &= \sin \phi \frac{\partial \tilde{S}_z^{\text{ADC}}}{\partial r} + \frac{1}{r} \cos \phi \frac{\partial \tilde{S}_z^{\text{ADC}}}{\partial \phi} \\
&= \sin \phi \frac{2(|l_2| - |l_1|)|v|^2}{r B_2^3} [(1 - 2\eta)B_2^2 + (2\eta - 1)^3 |v|^4 - 2(2\eta - 1)(\eta - 1)|v|^2 - 1],
\end{aligned} \tag{S65}$$

where $B_2^2 = (1 + |v|^2)^2 - 4\eta(1 - \eta)|v|^4$. By using the Eq. (S2), we get the z th component of the field

$$\Sigma_z^{\text{ADC}} = \frac{4\Delta l (|l_2| - |l_1|)|v|^2}{r^2} \cdot \frac{\eta[1 + (2\eta - 1)|v|^2]}{[(1 + |v|^2)^2 - 4\eta(1 - \eta)|v|^4]^{3/2}}, \tag{S66}$$

and then the skyrmion number is

$$N_z^{\text{ADC}} = \begin{cases} \Delta l, & \frac{1}{2} < \eta \leq 1 \\ 0, & 0 \leq \eta < \frac{1}{2} \end{cases} \tag{S67}$$

where $\eta \neq \frac{1}{2}$ in Eq. (S67).

Different initial scale coefficients (a, b) and corresponding skyrmion numbers

An initial state of the system is $|\Psi\rangle = a|l_1\rangle|0\rangle + b|l_2\rangle|1\rangle$, ($a \neq 0, b \neq 0$) and the scale coefficients (a, b) can vary prompting different initial concurrence values under the condition of normalization (i.e. $|a|^2 + |b|^2 = 1$). However, different values of a and b do not influence the trend of skyrmion numbers, regardless of the presence or absence of local decoherence.

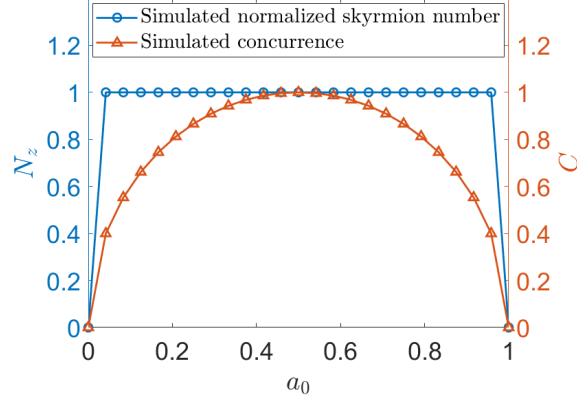


FIG. S1. The simulated normalized skyrmion numbers and concurrence values vary with scale coefficient a_0 in the case of no decoherence.

Firstly, we examine the case without decoherence in Fig. S1. Here, $a = \sqrt{a_0}$ and $b = \sqrt{1 - a_0}$. By varying a_0 , we obtain different initial states. However, the skyrmion numbers remain topologically stable and unchanged unless the degree of entanglement vanishes. This result is consistent with the one in Ref. [42].

Secondly, in the main text, we study the case of maximum entanglement degree (concurrence $C = 1$) with the presence of local decoherence channels. In Fig. S2 and S3, the scale coefficients are $a_0 = 1/4$ and $a_0 = 1/10$, respectively. But different initial states have the same results so that each critical transition point of skyrmion numbers in local decoherence is impervious.

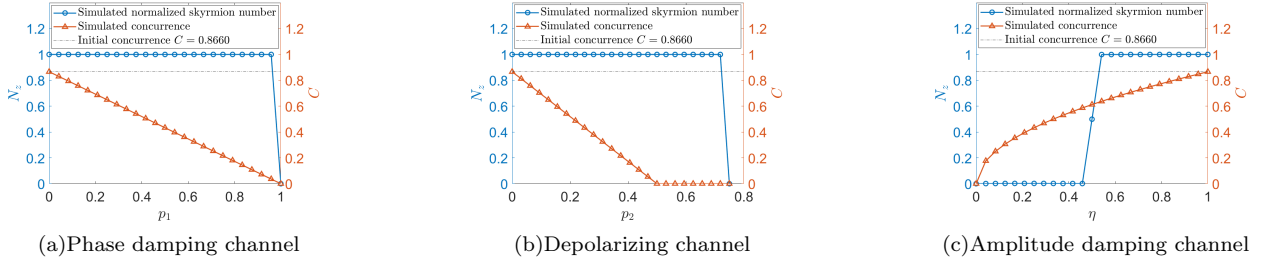


FIG. S2. The simulated normalized skyrmion numbers and concurrence values in different local decoherence channels. The scale coefficients $a_0 = 1/4$, $a = 1/2$ and $b = \sqrt{3}/2$ correspond to an initial concurrence of $C = 0.8860$.

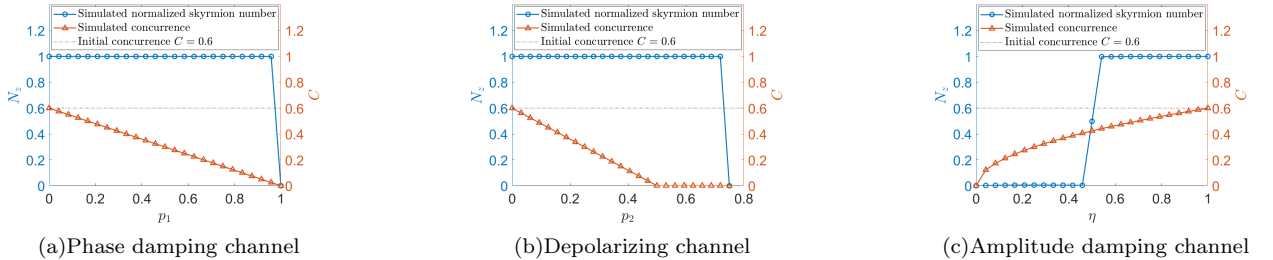


FIG. S3. The simulated normalized skyrmion numbers and concurrence values in different local decoherence channels. The scale coefficients $a_0 = 1/10$, $a = 1/\sqrt{10}$ and $b = 3/\sqrt{10}$ correspond to an initial concurrence of $C = 0.6$.

In addition, in the main text, we take two LG modes with azimuthal indices ($l_1 = 8, l_2 = 0$) as an example to interpret skyrmions' properties. In Fig. S4, we make a smaller value $N_z = 2$ with ($l_1 = 2, l_2 = 0$), and the features of skyrmions are all the same.

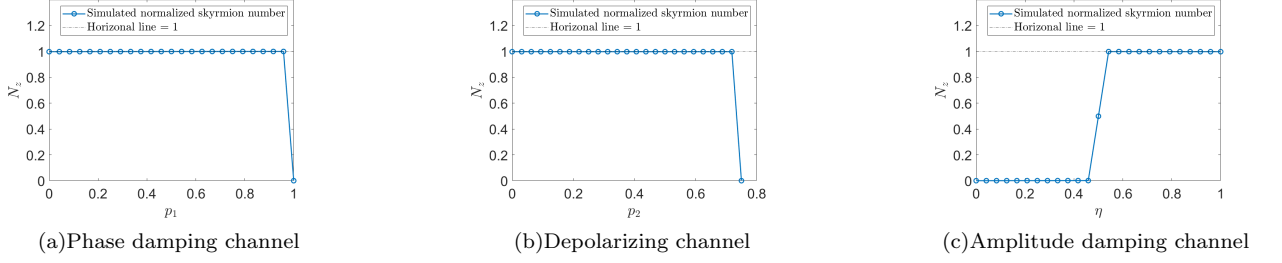


FIG. S4. The simulated normalized skyrmion numbers in different local decoherence channels. The azimuthal indices of two spatial modes are $l_1 = 2$ and $l_2 = 0$. The scale coefficients $a_0 = 1/2$, $a = 1/\sqrt{2}$ and $b = 1/\sqrt{2}$ correspond to an initial concurrence of $C = 1$.

The Stokes parameters vary with the decoherence strength

An ordinary state is usually denoted by a density matrix ρ which can be expanded using the identity \mathbb{I} and three Pauli matrices σ . For a 2D density matrix, it can be expressed by $\rho = \frac{1}{2}(\mathbb{I} + \mathbf{n} \cdot \sigma)$, and the vector $\mathbf{n} = (n_x, n_y, n_z) = |\mathbf{n}|(\sin \theta \cos \phi, \sin \theta \sin \phi, \cos \theta)$, (where $\theta \in [0, \pi]$, $\phi \in [0, 2\pi]$), is called the Bloch vector pointing in the spin direction. Actually, the 3D Stokes parameters $\mathbf{S}(\mathbf{r})$ equivalently represent the spin vector direction in the Bloch sphere. We numerically demonstrate the variations of the Stokes parameters with different decoherence strength. Taking a slice of azimuthal angle $\phi = 0$ (i.e. $S_y = 0$) as an example, we observe the curves in Fig. S5, S6, S7. In Fig. S5, the z component of the Stokes parameters, S_z , remains invariant yet the x component of the Stokes parameters S_x is fading and eventually $S_x = 0$, resulting in complete decoherence. In Fig. S6, as the decoherence strength increases, both S_x and S_z decrease until they reach zero. In Fig. S7, S_x gradually decreases with increasing decoherence strength of amplitude damping channel, while S_z becomes unable to reach the upper hemisphere when the damping factor $\eta \leq \frac{1}{2}$.

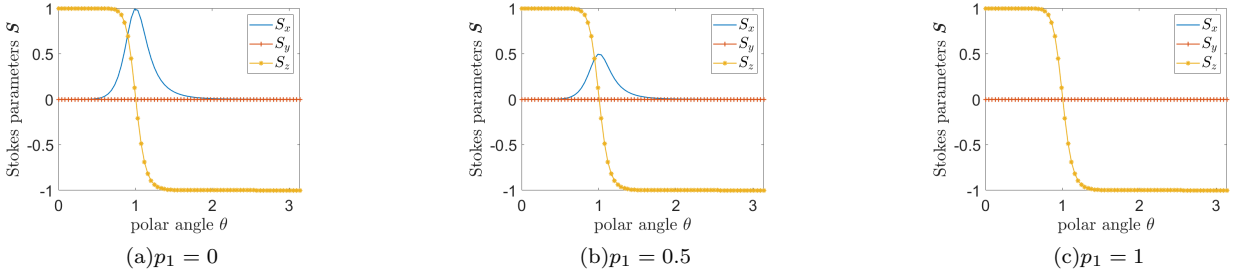


FIG. S5. The Stokes parameters $(S_x, S_y, S_z)(\mathbf{r})$ vary with different decoherence strength ($p_1 = 0, p_1 = 0.5, p_1 = 1$) of phase damping channel. We choose a slice of $S_y = 0$ as an example.

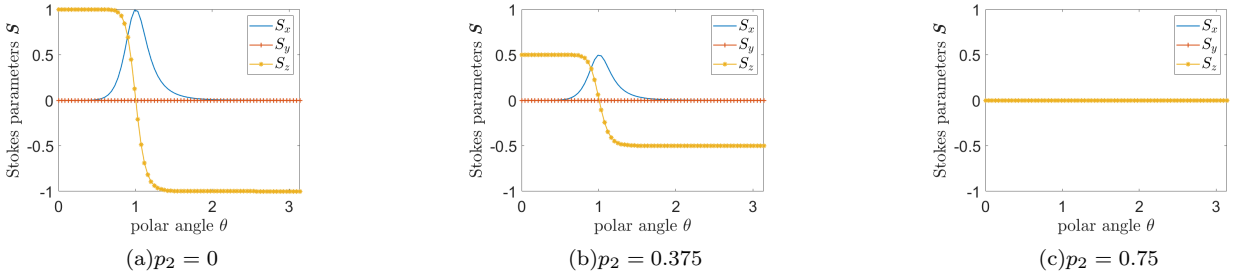


FIG. S6. The Stokes parameters $(S_x, S_y, S_z)(\mathbf{r})$ vary with different decoherence strength ($p_2 = 0, p_2 = 0.375, p_2 = 0.75$) of depolarizing channel. We choose a slice of $S_y = 0$ as an example.

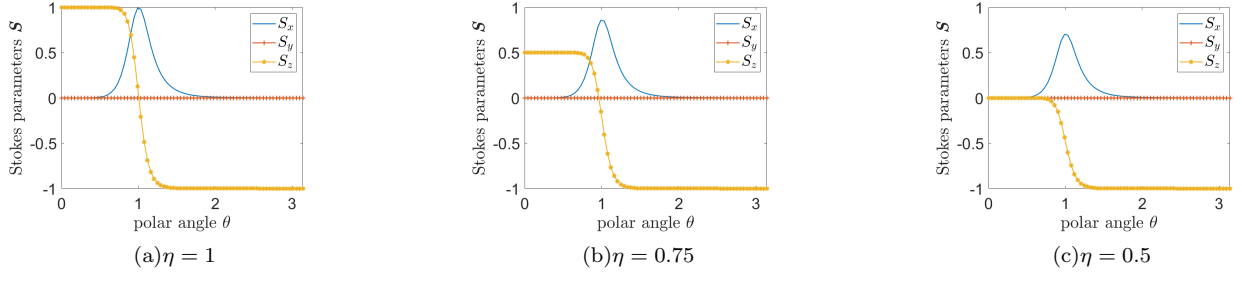


FIG. S7. The Stokes parameters $(S_x, S_y, S_z)(\mathbf{r})$ vary with different decoherence strength ($\eta = 1, \eta = 0.75, \eta = 0.5$) of amplitude damping channel. We choose a slice of $S_y = 0$ as an example.

Entanglement sudden death (ESD)

The interaction between two entangled qubits and the surrounding noisy environment may provoke the dissipation or/and dephasing effects and even the loss of quantum correlation. Quantum correlation can be quantified by the concurrence C which varies between $C = 0$ of classical correlation and $C = 1$ of maximal entanglement. The expression of concurrence is $C(\rho) = \max\{0, \sqrt{\lambda_1} - \sqrt{\lambda_2} - \sqrt{\lambda_3} - \sqrt{\lambda_4}\}$ and $\lambda_i (i = 1, 2, 3, 4)$ are the positive eigenvalues in decreasing order of the operator $R = \rho(\sigma_y \otimes \sigma_y)\rho^*(\sigma_y \otimes \sigma_y)$ [54]. We generally use the term ‘decoherence’ to describe the decay and loss of quantum correlation or entanglement and there is some research that shows only local decoherence is sufficient to lead to ESD [54, 60, 61]. ESD is a phenomenon that entanglement of a system vanishes in a finite time and it is different from the asymptotic decay in a infinite time. For three decoherence channels, there are distinct features.

In phase damping channel, the concurrence conforms to $C(\rho_{out}) = 2|a||b|(1 - p_1)$. When $p_1 = 1$, the density matrix corresponds to the maximally mixed state and the entanglement completely vanishes.

In depolarizing channel, the final density matrix is in the Eq. (S38) and the upper bound of p_2 is $\frac{3}{4}$. The depolarizing channel with $p = 3/4$ can map any input to the maximally mixed state. The concurrence is $C(\rho_{out}) = \max\{2|a||b|(1 - 2p_2), 0\}$. When $p_2 = 1/2$, the concurrence is zero, which reveals the occurrence of ESD.

In amplitude damping channel, from the Eq. (S52), the atom always stays at the ground state if $\eta = 0$. The concurrence in amplitude damping channel is $C(\rho_{out}) = 2|a||b|\sqrt{\eta}$, showing no ESD as entanglement does not completely vanish until $\eta = 0$.

Obviously, depolarizing noise can cause finite-time entanglement decay yet phasing noise and amplitude noise have no ESD.

The skyrmion numbers in loss

When we consider the loss of two polarization components of the optical skyrmion field, there are two types of possible cases, i.e., the equal loss parameters and unequal loss parameters. The unnormalized state is expressed as

$$|\Psi\rangle = aT_a |l_1\rangle |0\rangle + bT_b |l_2\rangle |1\rangle, \quad (\text{S68})$$

where $T_a \in [0, 1]$ and $T_b \in [0, 1]$ are the loss parameters of two components, respectively. $T_a = 1$ and $T_b = 1$ indicate no loss and $T_a = 0$ (or $T_b = 0$) means the skyrmion number of the field is zero. Similarly, we can calculate the corresponding skyrmion numbers by Eq. (S3).

If $T_a = T_b \neq 0$, the normalized state is

$$|\Psi\rangle_{\text{Loss}}^{\text{equal}} = c_1 a T_a |l_1\rangle |0\rangle + c_1 b T_b |l_2\rangle |1\rangle. \quad (\text{S69})$$

The output density matrix is

$$\begin{aligned} \rho_{\text{Loss}}^{\text{equal}} &= |c_1|^2 [|a|^2 T_a^2 |l_1\rangle \langle l_1| \otimes |0\rangle \langle 0| + ab^* T_a T_b |l_1\rangle \langle l_2| \otimes |0\rangle \langle 1| \\ &\quad + a^* b T_a T_b |l_2\rangle \langle l_1| \otimes |1\rangle \langle 0| + |b|^2 T_b^2 |l_2\rangle \langle l_2| \otimes |1\rangle \langle 1|] \\ &= |c_1|^2 T_a^2 [|a|^2 |l_1\rangle \langle l_1| \otimes |0\rangle \langle 0| + ab^* |l_1\rangle \langle l_2| \otimes |0\rangle \langle 1| \\ &\quad + a^* b |l_2\rangle \langle l_1| \otimes |1\rangle \langle 0| + |b|^2 |l_2\rangle \langle l_2| \otimes |1\rangle \langle 1|], \end{aligned} \quad (\text{S70})$$

where $c_1 = \frac{1}{T_a}$ is the normalized coefficient. Comparing Eq. (S70) with Eq. (S5), they differ only by a factor $|c_1|^2 T_a^2 = 1$ that has no impact on computing the locally normalized Stokes parameters in Eq. (S18-S20). Thus, the skyrmion number remains constant when the two polarization components have equal loss parameters unless $T_a = T_b = 0$.

If $T_a \neq T_b$ and $T_a \neq 0, T_b \neq 0$, the normalized state is

$$|\Psi\rangle_{\text{Loss}}^{\text{unequal}} = c_2 a T_a |l_1\rangle |0\rangle + c_2 b T_b |l_2\rangle |1\rangle. \quad (\text{S71})$$

the output density matrix is

$$\begin{aligned} \rho_{\text{Loss}}^{\text{unequal}} &= |c_2|^2 [|a|^2 T_a^2 |l_1\rangle \langle l_1| \otimes |0\rangle \langle 0| \\ &\quad + ab^* T_a T_b |l_1\rangle \langle l_2| \otimes |0\rangle \langle 1| \\ &\quad + a^* b T_a T_b |l_2\rangle \langle l_1| \otimes |1\rangle \langle 0| \\ &\quad + |b|^2 T_b^2 |l_2\rangle \langle l_2| \otimes |1\rangle \langle 1|] \\ &= \sum_{pqst=1}^2 \mu_{pqst}'''' |l_p\rangle \langle l_q| \otimes |e_s\rangle \langle e_t|, \end{aligned} \quad (\text{S72})$$

where $c_2 = \sqrt{\frac{1}{T_a^2 |a|^2 + T_b^2 |b|^2}}$ is the normalized coefficient. We can rewrite the normalized state in Eq. (S71) using new coefficients a' and b' , i.e.,

$$|\Psi\rangle_{\text{Loss}}^{\text{equal}} = a' |l_1\rangle |0\rangle + b' |l_2\rangle |1\rangle, \quad (\text{S73})$$

where $a' = \frac{T_a a}{\sqrt{T_a^2 |a|^2 + T_b^2 |b|^2}}$, $b' = \frac{T_b b}{\sqrt{T_a^2 |a|^2 + T_b^2 |b|^2}}$ and $|a'|^2 + |b'|^2 = 1$. Eq. (S73) is equivalent to the state $|\Psi\rangle = a |l_1\rangle |0\rangle + b |l_2\rangle |1\rangle$. $|e_1\rangle = |0\rangle$, $|e_2\rangle = |1\rangle$, $\mu_{1111}'''' = |c_2|^2 T_a^2 |a|^2 = |a'|^2$, $\mu_{1212}'''' = |c_2|^2 T_a T_b a b^* = a' b'^*$, $\mu_{2121}'''' = |c_2|^2 T_a T_b a^* b = a'^* b'$, $\mu_{2222}'''' = |c_2|^2 T_b^2 |b|^2 = |b'|^2$, and other coefficients are zero. Thus the skyrmion number in this case exhibits the same stability as in the case of the pure state without decoherence in Sec. , i.e., the skyrmion number remains stable unless the degree of entanglement vanishes ($a' = 0$ or $b' = 0$) described by Ref. [42].

Generation of inhomogeneous yet continuous decoherence channels

To generate a decoherence channel with a spatially distributed yet continuous damping factor, we control the correlation length ϵ of distribution and use the Fourier transform method [58, 62]. Considering a screen size of $N \times N$ (with $N = 1024$), we first create a Gaussian complex random matrix of size $M \times M$ (with $M = N/\epsilon$), filling the elements of $(1 : M, 1 : M)$. Then, we apply the Fourier transform to the entire matrix and finally obtain the modulus squared of the matrix as the desired result. For example, in Fig. S8, S9, S10, we demonstrate several inhomogeneous distributions of the damping factors in three local decoherence scenarios with different correlation lengths.

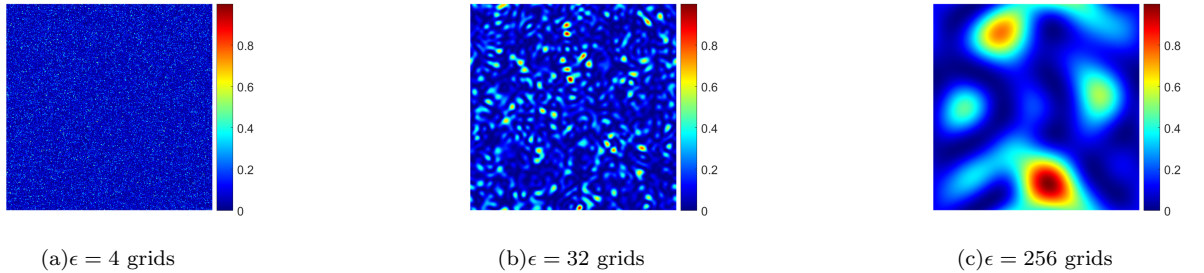


FIG. S8. Phase damping channel. The numerical screen size of grid is 1024×1024 , and we create three spatial distributions of the damping factor p_1 with different correlation lengths ($\epsilon = 4, 32, 256$ grids) as examples. $p_1(\mathbf{r}) \in [0, 1)$.

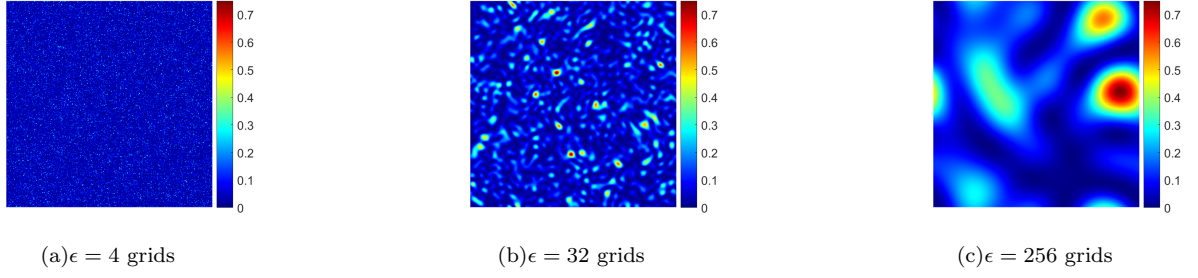


FIG. S9. Depolarizing channel. The numerical screen size of grid is 1024×1024 , and we create three spatial distributions of the damping factor p_2 with different correlation lengths ($\epsilon = 4, 32, 256$ grids) as examples. $p_2(\mathbf{r}) \in [0, \frac{3}{4}]$.

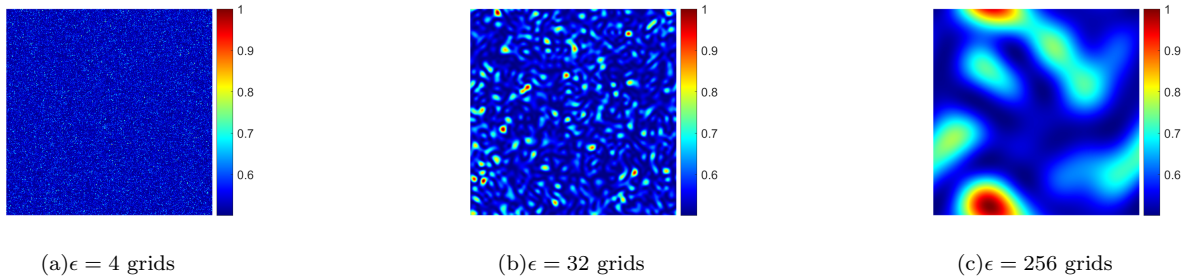


FIG. S10. Amplitude damping channel. The numerical screen size of grid is 1024×1024 , and we create three spatial distributions of the damping factor η with different correlation lengths ($\epsilon = 4, 32, 256$ grids) as examples. $\eta(\mathbf{r}) \in (\frac{1}{2}, 1]$.